ACS OMEGA

Open Access

http://pubs.acs.org/journal/acsodf

Article

Synthesis and Biological Evaluation of Benzothiazolyl-pyridine Hybrids as New Antiviral Agents against H5N1 Bird Flu and SARS-COV-2 Viruses

Nadia Hanafy Metwally,* Galal Hamza Elgemeie, and Fatma Gomaa Fahmy

Cite This: *ACS Omega* 2023, 8, 36636−36654

Read Online

ACCESS | Metrics & More | Article Recommendations | Supporting Information

ABSTRACT: A novel series of benzothiazolyl-pyridine hybrids **8a−h** and **14a−e** were produced from the reaction of enamine derivative **4** with each of the arylcyanoacetamides **5a−h** and cyanoacetohydrazides **9a−e**. The new products were characterized by spectral techniques (IR, ^{1}H NMR, ^{13}C NMR, and MS). Biological evaluation of **8a−h** and **14a−e** in *vitro* against H5N1 and SARS-COV-2 viruses showed that several compounds had significant activity. Compounds **8f−h**, which contain fluorine atoms, have better activity against H5N1 and anti-SARS-CoV-2 viruses than the other compounds included in this study. Compound **8h** has a trifluoromethyl group at position-3 of the phenyl ring and exhibits a high activity against H5N1 virus with 93 and 60% inhibition at concentrations of 0.5 and 0.25 μmol/μL, respectively, among the tested compounds, and it also showed anti-SARS-CoV-2 virus with a half-maximum inhibition rate of 3.669 μM, among the remaining compounds. The mechanism of action of **8f−h**, which is expected to be repurposed against COVID-19, was investigated. The results showed that the compounds have virucidal effects at different stages of the three mechanisms of action. Furthermore, compounds **8f−h** were found to possess CoV-3CL protease inhibitory activities with IC_{50} values of 544.6, 868.2, and 240.6 μg/mL, respectively, compared to IC_{50} = 129.8 μg/mL of the standard drug lopinavir. Interestingly, compounds **8f−h** also showed high inhibitory activity against the H5N1 virus as well as the SARS-CoV-2 virus. Moreover, compounds **8f−h** fit admirably into the active site of the SARS-CoV-2 main protease (PDB ID: 6LU7) using the molecular docking Moe software 2015.10.

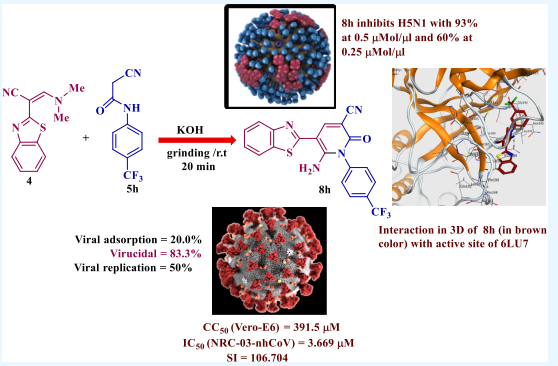

1. INTRODUCTION

Influenza, corona, and other related pneumotropic viruses cause illness and death by inducing an excessive inflammatory immune response in the host's airways.

Influenza A viruses are classified into subtypes according to two proteins present on the virus surface. Hemagglutinin (HA), which promotes receptor binding and membrane fusion, and neuraminidase (NA), which helps in the release of viral progeny.[1] Subtypes of influenza A include H1N1, H2N2, H3N2, H5N1, H7N7, and H9N2, which can be isolated from humans, suggesting that human host constraints as a virus have been suggested.[2] There are two types of H5N1: highly pathogenic (HPAI), commonly referred to as "Bird flu" (HPAI), and low pathogenic. In 1997, there were few cases of H5N1 infection between chickens and humans in Hong Kong, but the number of infected people increased until outbreaks were reported in several Asian countries in 2004 and 2005, and these outbreaks were slow to subside. In 2006, the total number of confirmed human cases of H5N1 had amounted to 174, of which 94 were fatal.[3] WHO confirmed 455 human death cases from 861 of total infected human cases since 2003−2020.[4] A human pandemic with H5N1 virus could potentially be catastrophic due to an almost complete lack of antibody-mediated immunity to the H5 surface protein in most human populations and the virulence of this viral subtype. Data also indicate that the H5N1 strain is particularly harmful due to it having 50% mortality rate in humans and is more likely to be transferred among humans than seasonal influenzas, which have a higher mortality rate.

Currently, anti-influenza drugs (H5N1) are classified into two classes, as shown in Figure 1. The first class is the M2 proton channel inhibitors like amantadine and rimantadine.[5,6] The second class is the neuraminidase inhibitors like oseltamivir, peramivir, and zanamivir (Figure 1).[7,8]

Meanwhile, the severe acute respiratory syndrome coronavirus (SARS-CoV-2) spread rapidly, causing a pandemic coronavirus infection 2019 (COVID-19). Since the first outbreak in Wuhan, China, in December 2019, according to the WHO, more than 760 million people worldwide of

Received: March 24, 2023
Accepted: August 18, 2023
Published: September 25, 2023

https://doi.org/10.1021/acsomega.3c01987
ACS Omega 2023, 8, 36636−36654

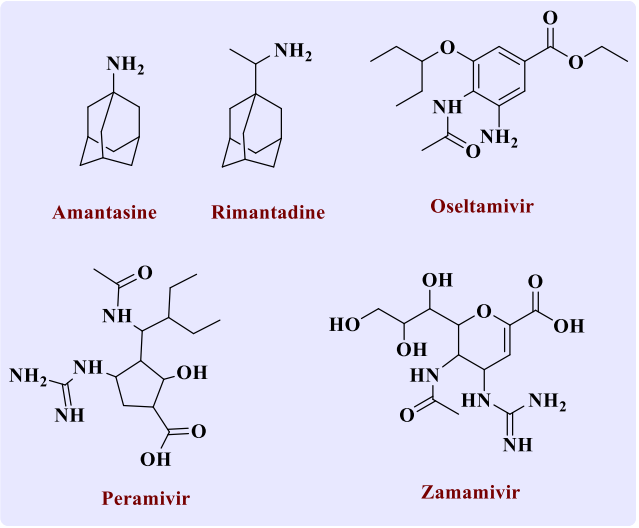

Figure 1. Approved drugs used for avian influenza A.

COVID-19 cases have been confirmed, and 6.8 million people have died. To date, SARS-CoV-2 is the most interesting topic in coronavirus infections. There are many potential candidates for therapeutics against this type of virus, including chloroquine,[9] hydroxychloroquine,[10] remdesivir,[11] and lopinavir/ritonavir[12] (Figure 2). Various phytochemicals were also utilized against SARS-CoV-2 virus such as flavone and coumarin derivatives,[13] theophyllines,[14] and saikosaponins.[15]

SARS-CoV-2 is composed of two overlapping polyproteins (pp1a and pp1ab) encoded in the RNA genome, whose cleavage is essential for replication and transcription processes.[15] These cleavage processes are mediated by the major protease M^{pro} (3-chymotrypsin-like protease 3CLpro) and nonstructural viral proteins such as the papain-like protease PLpro.[16−19] In this regard, inhibition of viral RNA synthesis is considered as one way to combat coronaviruses.[20]

According to reports, influenza A and COVID-19 are both contagious respiratory diseases, although caused by different viruses. Influenza is caused by infection with the influenza virus, whereas COVID-19 is caused by infection with a coronavirus (SARS-CoV-2), which was first discovered in 2019. Avian influenza A (H5N1) and COVID-19 have similar symptoms including fever, muscle aches, headache, sneezing, and coughing.[21,22] However, despite similar disease symptoms, influenza viruses and COVID-19 contrast in terms of replication, immune stimulation, and overall fatality.[23] Moreover, some clinical and laboratory findings have been reported to be similar for both infection in patients with influenza and COVID-19 coinfection, making the diagnoses of these coinfected patients difficult. For suspected patients, detection methods specific for influenza virus and SARS-V-2 are recommended.[24]

In addition, there are prominent antiviral drugs containing pyridine and dihydropyridine cores such as dorvirine, which is considered a nonnucleoside reverse transcriptase inhibitor and is used to treat HIV infection.[25] Tipranavir, which contains the trifluoromethyl group is used also as an anti-HIV drug and in combination with ritonavir used as a combination medicine.[26] Baloxavir marboxil drug is used as a treatment for influenza A and influenza Bird flu[27] (Figure 3). Compound **I** has been reported to have low toxicity with high activity against the H5N1 influenza[28] (Figure 3). Moreover, a natural product with 2-pyridine scaffold has been used as a therapeutic agent against the novel coronavirus SARS-CoV-2.[29]

Compounds containing the benzothiazole moiety demonstrated to exhibit antiviral activity.[30] For example, frentizole (benzothiazolyl urea derivative) **II** is used as an HSV and immunosuppressive agent,[31] as shown in Figure 3. The bis-tetrahydrofuranyl-urethane analogue of benzothiazole **III** is used as an HIV as well as in phase-3-ongoing COVID-19 (Figure 3).[32] It is worth noticing that joining two or more diverse heterocyclic rings into one structure may bring about new compounds with upgraded bioactivity.[33] As an example, pyridines with the benzothiazole moiety have enhanced

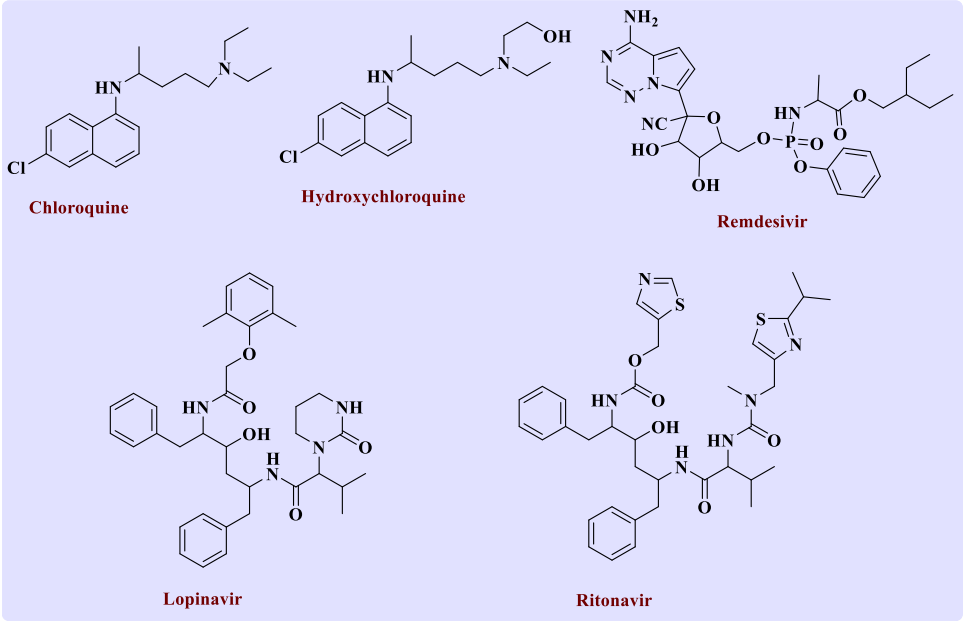

Figure 2. Structures of some drugs used as anti-COVID-19.

https://doi.org/10.1021/acsomega.3c01987
ACS Omega 2023, 8, 36636−36654

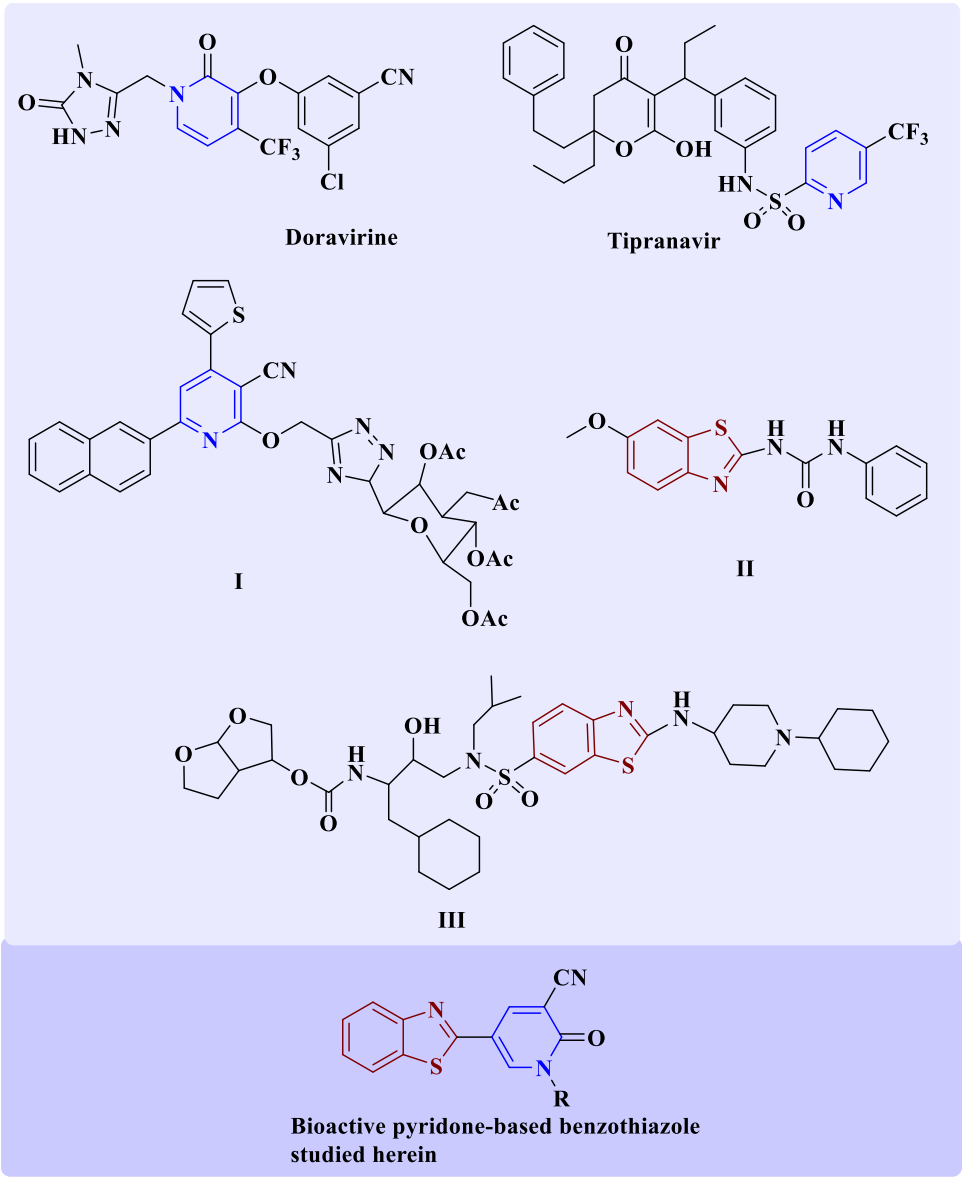

Figure 3. Structures of antiviral market drugs containing pyridine and benzothiazole and our targets present in the current study.

antibacterial and antifungal activities.[34,35] To achieve this goal, new strategies for synthesizing pyridine-bearing benzothiazole moieties have been generated.[36−39] As a continuation of our previous work on the synthesis of bioactive heterocyclic ring systems,[40−54] we herein report that the cytotoxic activity of some novel arylpyridines incorporated benzothiazole moieties **8a−h** against H5N1, SARS-COV-2 viruses, and their inhibition of SARS-COV-2 main protease (M^{pro}). Molecular docking studies of more potent main protease inhibitors were also performed to find a potential candidate as antiviral agent toward H5N1 and SARS-CoV-2 viruses.

2. RESULTS AND DISCUSSION

2.1. Chemistry. The starting 2-cyanomethylbenzothiazole **3** was synthesized from the grinding of *o*-aminothiophenol **1** and malononitrile **2** using lemon juice as a natural acid catalyst at room temperature for 30 min as well as the conventional method,[55] as shown in Scheme 1.

Furthermore, the enamine derivative **4**[56] was prepared from grinding compound **3** with *N,N*-dimethylformamide dimethyl acetal (DMF-DMA) at ambient temperature for 10 min, as depicted in Scheme 2.

Scheme 1. Synthesis of 2-Cyanomethylbenzothiazole 3

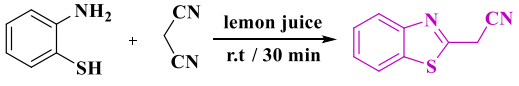

1 2 3

Scheme 2. Synthesis of Enamine Derivative 4

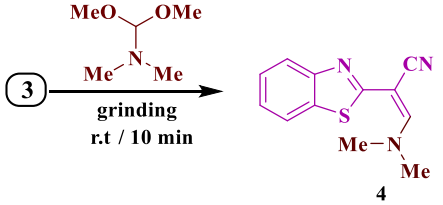

4

https://doi.org/10.1021/acsomega.3c01987
ACS Omega 2023, 8, 36636−36654

Scheme 3. Synthesis of 5-(Benzothiazolyl)-1-(aryl)-pyridine-2-ones 8a−h

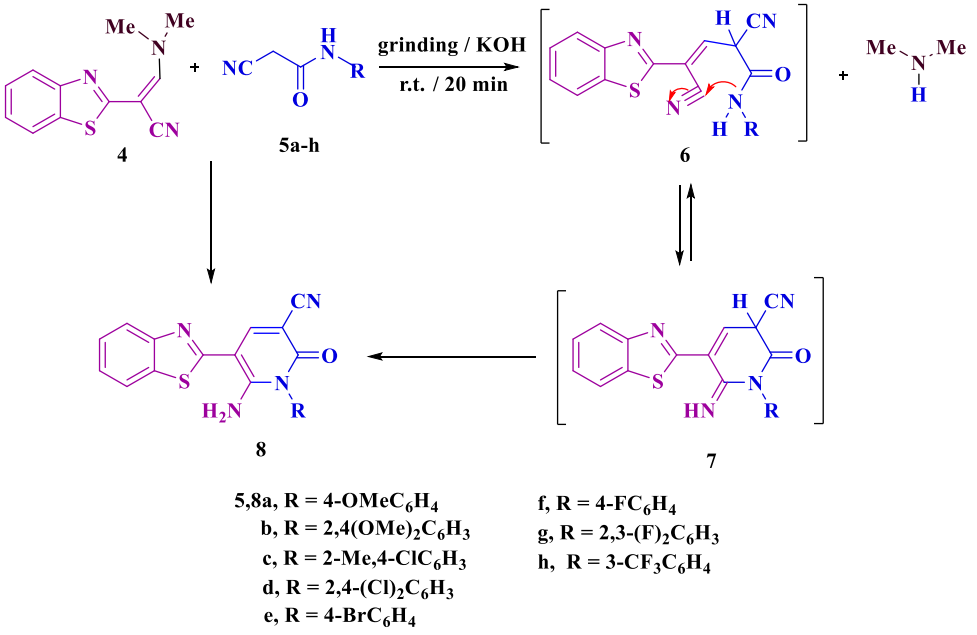

Scheme 4. Synthesis of Benzothiazolyltriazolo[1,5-*a*]pyridine Derivatives 14a−e

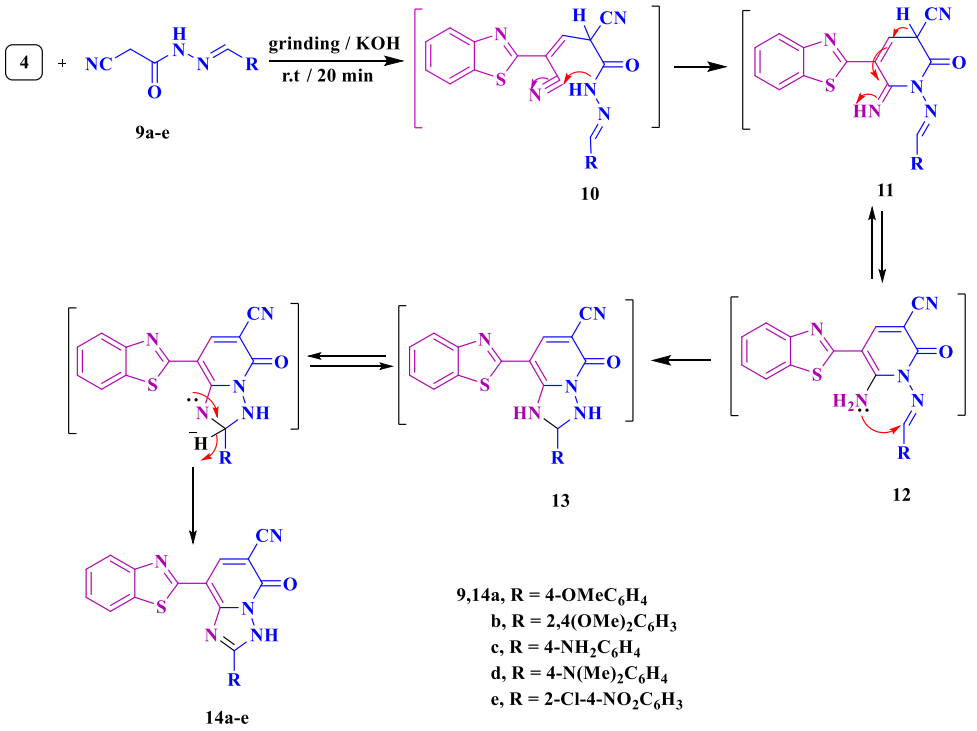

On the other hand, grinding of equimolar amounts of compound **4**, *N*-aryl-2-cyanoacetamides **5a−h**, and potassium hydroxide in a mortar at room temperature for 20 min gave the new *N*-substituted 2-pyridyl benzothiazoles **8a−h**, as shown in Scheme 3 and Figure 6. Their essential examination, such as spectral data, confirmed the obtainable products **8a−h**. For illustration, the ^{1}H NMR spectrum of compound **8b** appeared with two singlet signals at δ = 3.75 and 3.86 ppm for the two methoxy protons, and another three doublets at δ = 7.66, 7.83, and 8.11 ppm with coupling constants J = 7.2, 8.4, and 7.2 Hz, respectively, due to the protons of aryl groups. Also, a peak at δ = 8.27 ppm for the pyridine proton showed up. The ^{13}C NMR spectrum of compound **8b** showed characteristic signals at 55.7 (OCH_3), 56.5 (OCH_3), 104.6 (CN), 149.5 (C−NH_2), 161.0 (CO), and 165.0 (C═N) ppm. In addition, other signals correspond to aryl carbons at 74.8, 76.8, 99.1, 120.1, 120.3, 120.5, 121.7, 122.9, 126.3, 144.4, and 155.0 ppm. The mass spectrum of compound **8b** contains molecular ion peaks at m/z = 404 (M^+, 100%), corresponding to the molecular formula $C_{21}H_{16}N_4O_3S$. The reaction mechanism was illustrated as the disposal of a dimethylamine molecule following *Michael* addition, and intramolecular cyclization was achieved by

https://doi.org/10.1021/acsomega.3c01987
ACS Omega 2023, 8, 36636−36654

adding an amino proton to the cyano group, followed by tautomerization forming 2-pyridyl benzothiazoles **8a−h**.

Additionally, grinding compound **4** with 2-cyano-*N*′-(4-substituted benzylidene) acetohydrazides **9a−e** in a mortar at room temperature for 20 min yielded compounds **14a−e**, as shown in Scheme 4. A fundamental investigation analysis of compounds **14a−e** was used to confirm the suggested structures. The IR spectrum of compound **14b** showed absorption bands at 3398, 2206, and 1612 cm^{-1} due to the NH, CN, and CO groups, respectively. The ^1H NMR spectrum of **14b** showed two singlet signals at δ = 3.85 and 3.91 ppm due to the two methoxy protons and another two doublet signals at δ = 7.90 and 8.04 with a coupling constant of J = 7.6 Hz, which demonstrated the aryl protons. A singlet signal at δ = 8.47 ppm was of the pyridine CH proton. Also, ^{13}C NMR affirmed the structure of compound **14b**, where the characteristic peaks appeared at δ = 56.0 (OCH_3), 57.2 (OCH_3), 114.7 (CN), 153.4 (C═N), 160.3 (C═N), and 163.0 (CO) ppm. Moreover, other signals due to aryl carbons at 81.1, 101.1, 116.6, 117.1, 120.4, 121.5, 121.8, 122.2, 123.8, 126.3, 135.0, 135.2, 152.1, and 152.9 ppm were presented. The proposed reaction pathway included the addition of the active methylene group of 2-cyano-*N*′-(4-substituted benzylidene)-acetohydrazides **9a−e** to the double bond of the beginning compound **4** to form intermediate **10**; *Michael* adduct with the consequent end of the dimethylamino group yielded intermediate **11**. Tautomerism of intermediate **11** happens to make intermediate **12**, via intramolecular cyclization, involving the bonding of the amino group to the C═N to give intermediate **13**, followed by autoxidation yielding the pyridone hybrids **14a−e**.

2.2. Biological Activity. *2.2.1. H5N1 Influenza Virus.* The MTT assay was used to determine the safe dose of each of the synthesized benzothiazolyl-pyridine derivatives **8a−h** and **14a−e**. From a linear equation generated for each compound, IC_{50} values are listed in Table 1. The antiviral activity of safe doses of each compound against H5N1 virus was investigated using a plaque reduction assay. The results demonstrated that compound **8h** (contains the 3-fluoromethyl group) exhibited the highest activity against H5N1 influenza virus strain among the tested derivatives where inhibition appeared at 93 and 60% at concentrations equal to 0.5 and 0.25 μmol/μL, respectively, compared to ribavirin as a broad-spectrum antiviral standard drug of 100% inhibition at concentration 0.5 μmol/μL and 86% inhibition at 0.25 μmol/μL. The following compounds **8f** (contains one fluoro group), **8g** (contains two fluoro groups), and **14d** (*N*,*N*-dimethyl groups) exhibited 88, 67, and 73% inhibition at 0.5 μmol/μL, respectively. Compound **14c** with an amino group also showed 65% inhibition at 0.25 μmol/μL. However, compounds **8e**, **14a**, and **14e** showed moderate antiviral activity against H5N1, with inhibition rates 47, 55, and 20% at concentration 0.25 μmol/μL, while **8a** (17%) and **8b** (7%) showed a very weak rate of inhibition at concentration 0.25 μmol/μL. Compound **8c**, with methyl and chloro groups at 2- and 4-positions in the phenyl ring, respectively, showed no cytotoxic activity against H5N1 among all tested compounds at any concentration (Figure 4). Some reports revealed that heterocyclic compounds with substituent methyl or chloro groups compared to other functional groups showed weak or no antiviral activity.[57,58]

2.2.2. Detection of In Vitro Cytotoxicity. The colorimetric MTT assay was used to assess the cytotoxicity of compounds **8a−h** and **14a−e** on Vero-E6 cells. The results showed that

Table 1. Antiviral Activities of All Synthesized Compounds

compound no	concentration (μmol/μL)	initial viral count	viral count (PFU/mL)	inhibition (%)
8a	0.5	5.2×10^{-6}	6×10^{-6}	13
	0.25	5×10^{-6}	6×10^{-6}	17
8b	0.5	5.5×10^{-6}	6×10^{-6}	8
	0.25	5.6×10^{-6}	6×10^{-6}	7
8c	0.5	unable	6×10^{-6}	0
	0.25	unable	6×10^{-6}	0
8d	0.5	3×10^{-6}	6×10^{-6}	60
	0.25	4.7×10^{-6}	6×10^{-6}	22
8e	0.5	2.3×10^{-6}	6×10^{-6}	52
	0.25	3.2×10^{-6}	6×10^{-6}	47
8f	0.5	0.7×10^{-6}	6×10^{-6}	88
	0.25	1.5×10^{-6}	6×10^{-6}	69
8g	0.5	2×10^{-6}	6×10^{-6}	67
	0.25	2.4×10^{-6}	6×10^{-6}	56
8h	0.5	5×10^{-6}	6×10^{-6}	93
	0.25	2.5×10^{-6}	6×10^{-6}	60
14a	0.5	2.4×10^{-6}	6×10^{-6}	60
	0.25	2.7×10^{-6}	6×10^{-6}	55
14b	0.5	2×10^{-6}	6×10^{-6}	67
	0.25	2.4×10^{-6}	6×10^{-6}	60
14c	0.5	3×10^{-6}	6×10^{-6}	50
	0.25	2×10^{-6}	6×10^{-6}	65
14d	0.5	1.6×10^{-6}	6×10^{-6}	73
	0.25	1.6×10^{-6}	6×10^{-6}	73
14e	0.5	3.6×10^{-6}	6×10^{-6}	40
	0.25	4.8×10^{-6}	6×10^{-6}	20
ribavirin	0.5	5×10^{-6}	6×10^{-6}	100
	0.25	2.8×10^{-6}	6×10^{-6}	86

CC_{50} and safety index (SI) of compounds **8a−h** ranged 1665−152 μM and 106.704−0.0487, respectively (Table 2, Figure 5). Compounds **14a−d**, on the other hand, exhibited CC_{50} and SI ranging 6276−143 μM and 14.897−0.0274, respectively (Table 2, Figure 6). The three best SARS-COV-2 inhibitors were **8f−g** with IC_{50} values of 10.52, 21.46, and 3.669 μM and SI values of 52.282, 115.971, and 106.704, respectively.

2.2.3. Anti-SARS-CoV-2 Activity. The inhibitory effects of compounds **8a−h** and **14a−e** on the SARS-COV-2 (NRC-03-nhCoV) virus in Vero-E6 cells were investigated. The results in Table 1 show that most of the compounds tested significantly inhibited the replication of the NRC-03-nhCoV virus in a dose-dependent profile. Compounds **8f−h** demonstrated superior inhibitory activity compared to compounds **14a−e** (Table 2 and Figure 5A and B). The most potent anti-SARS-COV-2 compound was **8f−h**, with IC_{50} values of 10.52, 21.46, and 3.669 μM, respectively. Compound **8a** (R = 4-methoxy as the donating group in the benzene ring) showed an IC_{50} value equal to 994.3 μM. Furthermore, insertion of another methoxy group at the 2-position of the benzene ring decreased the IC_{50} by 3.13-fold in IC_{50} as in the case of **8b** (IC_{50} = 3120 μM). The introduction of the withdrawing group such as the chlorine atom at the 4-position of the benzene ring improved the antiviral activity as in the case of **8c** (IC_{50} = 142.2 μM), while the insertion of another group of a chlorine atom at the 2-position of the benzene ring decreased the antiviral activity again as in **8d** (IC_{50} = 1596 μM). Changing the chlorine atom at position-4 of the benzene ring to a bromine atom increased the IC_{50} by 1.92-fold compared to **8c** (IC_{50} = 73.84 μM). Furthermore, since fluorine-containing drugs have become one

https://doi.org/10.1021/acsomega.3c01987
ACS Omega 2023, 8, 36636−36654

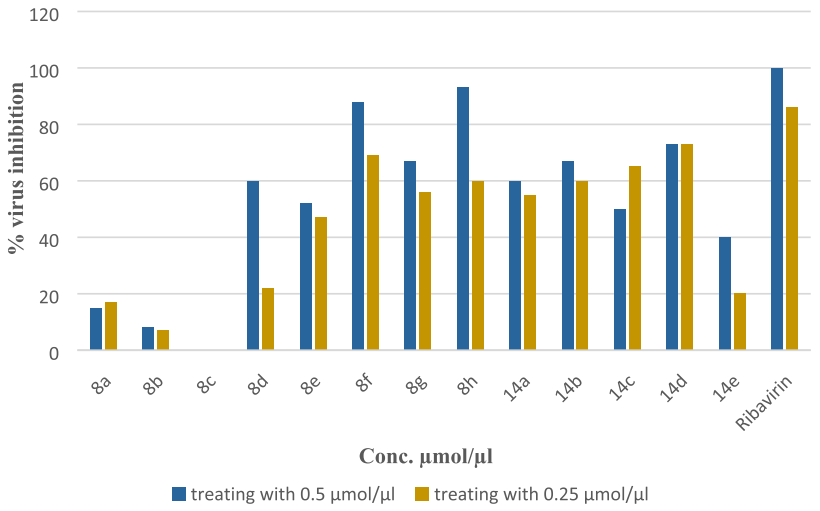

Figure 4. Antiviral activities of all synthesized compounds against H5N1.

Table 2. Anti-SARS-CoV-2 Activities of Compounds 8a−h

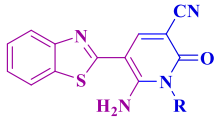

8a-h

compound no.	R	[a]CC_{50} (Vero-E6) μM	[b]IC_{50} (NRC-03-nhCoV) μM	[c]SI
8a	4-$OMeC_6H_4$	1651	994.3	1.660
8b	2,4-$(OMe)_2C_6H_3$	152	3120	0.0487
8c	2-Me-4-ClC_6H_3	1665	142.2	11.645
8d	2,4-$Cl_2C_6H_3$	1593	1596	0.998
8e	4-BrC_6H_4	1279	73.84	17.321
8f	4-FC_6H_4	550	10.52	52.281
8g	2,3-FC_6H_3	425.8	21.46	115.971
8h	3-$CF_3C_6H_4$	391.5	3.669	106.704

[a]CC_{50}. [b]IC_{50} values were derived from results of at least two independent experiments in Vero cells infected with SARS-CoV-2. [c]SI (Selective index) = CC_{50}/IC_{50} for inhibitory SARS-CoV-2 infection.

of the essential structural features in modern pharmaceuticals, the introduction of a fluorine atom in place of chlorine or bromine increases the antiviral activity, as in the case of compound **8f**, which contains one fluorine atom at the 4-position of the benzene ring, decreased the IC_{50} value to 10.520 μM and SI = 0.05228 as shown in Table 2. On the other hand, adding another fluorine atom at the 2-position of the benzene ring decreased the activity to IC_{50} = 21.46 μM as in the case of **8g**, but increasing the number of fluorine atoms as the trifluoromethyl group at the 3-position of the benzene ring (**8h**) resulted in a decrease of at least 2.86-fold in IC_{50} value (3.669 μM) compared to **8f** and 5.84-fold in IC_{50} value compared to **8g**, suggesting that the significance of the trifluoromethyl group (withdrawing group) is important for the SARS-COV-2 replication inhibitory activity in Vero-E6 cells.

In the second series, **14a−e**, compound **14b** (R = 2,5-dimethoxyphenyl) exhibited some activity against SARS-CoV-2 with IC_{50} = 70.48 μM, while the other tested compounds in this series showed weak activity (Table 3 and Figure 6A and B).

2.2.4. Mechanism of Anti-SARS-CoV-2 Activity. The inhibition rates for different mechanisms of action (virus adsorption, replication, and virucidal) of the most active compounds **8f−h** are shown in Table 4. The data depicted in this table show that compound **8f**, which contains one fluorine atom, decreases in concentration to $^1/_{100}$ and reduces virucidal inhibition by about 50%. However, adsorption and replication varied in both cases from 28.6 to 8.3%, and the concentration had no impact on inhibition. On the other hand, the adsorption rate of compound **8g** decreases with decreasing concentration, but in viral replication, concentration does not affect the inhibition rate (60%, 60%, and 53%). With compound **8h**, a precise effect on adsorption and viral replication appeared; both compounds **8g** and **8h** showed equally good results in virucidal properties, which were not affected by decreasing concentration. Thus, compound **8g** showed 80, 76.7, and 73.3% virucidal efficacy at concentrations of 10, 1, and 0.1 μM, respectively, while compound **8h** exhibited 83.3, 80, and 73.3% virucidal efficacy at concentrations of 10, 1, and 0.1 μM, respectively. Thus, in the three stages of compounds, **8f−h** exhibited multiple inhibitory effects, but the potency of their activity was mainly virucidal effect (Table 4 and Figure 7).

2.2.5. Inhibitory Activity against SARS-CoV-2 M^{pro}. The Protein Data Bank currently contains several potential target

https://doi.org/10.1021/acsomega.3c01987
ACS Omega 2023, 8, 36636−36654

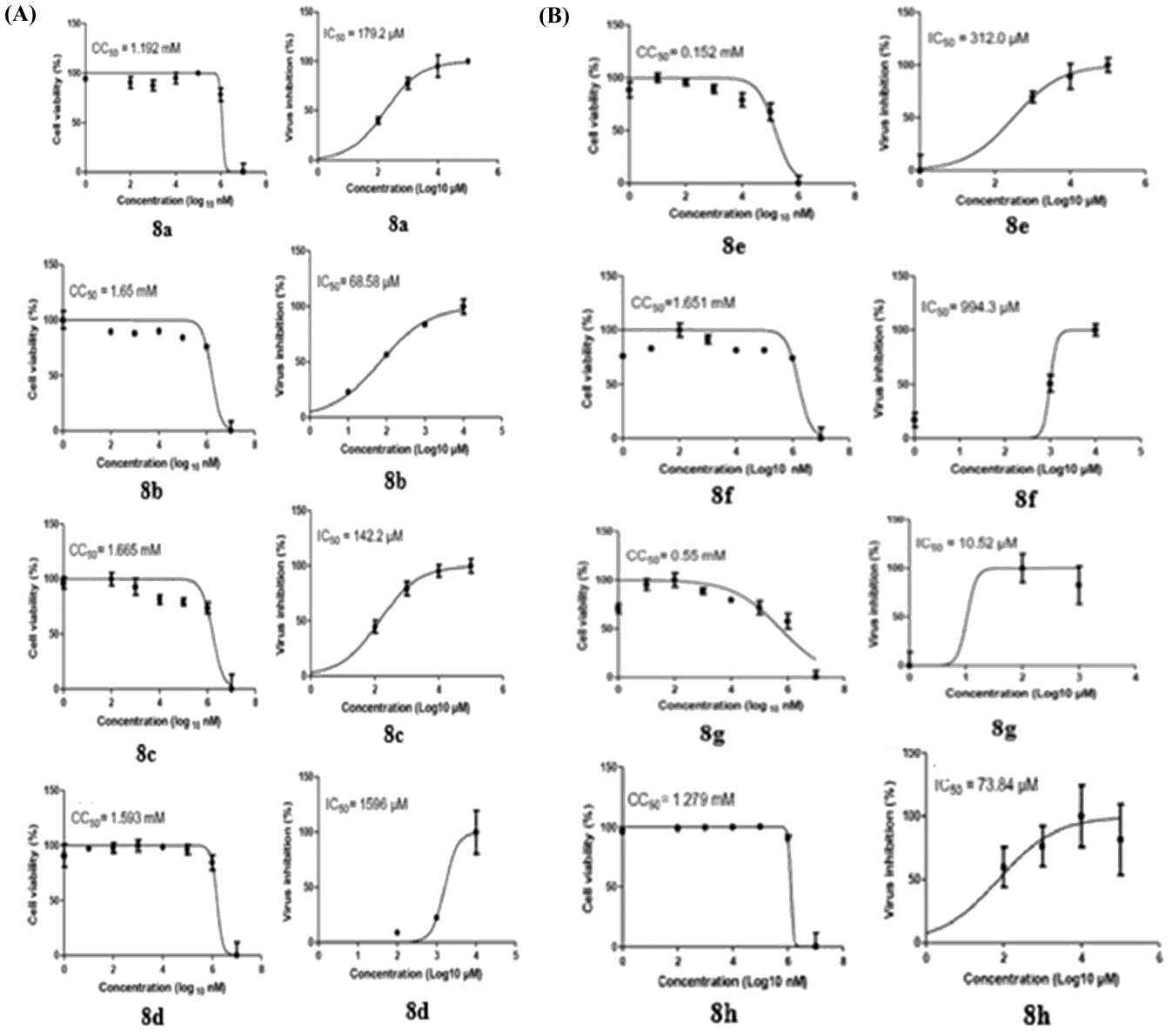

Figure 5. CC_{50} (50% cytotoxic concentration) of the tested *N*-pyridones in Vero-E6 cells and IC_{50} (50% inhibitory concentration) against the NRC-03-nhCoV virus in Vero-E6 cells (A and B). The CC_{50} and IC_{50} were plotted for each tested compound using Graph Pad Prism and were calculated from the nonlinear regression curve-fit analysis, relative to the virus and cell controls. The compounds **8a−h** exhibited antiviral activity against the NRC-03-nhCoV virus in Vero-E6 cells with IC_{50} ranging from 3.669 to 3120 μM. The most active compound is **8h** with IC_{50} = 3.669 μM and SI = 106.704 compared to the weakest compound **8b** with IC_{50} = 3120 μM and SI = 0.0487 in this series.

proteins isolated from coronaviruses (COVID-19). One of these crucial proteins, a protease, has been targeted by a panel of inhibitors with various chemical scaffolds, suggesting the potential for the creation of drugs against this challenging virus.[59,60] It is interesting to note that this enzyme and the comparable human proteases have completely different cleavage specificities, which makes it an excellent antiviral target with great selectivity and safety margins.[61] It was interesting in view of these to investigate the potential protease inhibitory effect of compounds **8f−h** against COVID-19. The inhibitory activities of compounds **8f−h** against SARS-CoV-2 Mpro were evaluated according to previously published procedure.[62] The results recorded in Table 3 indicated that the biological activity of these compounds depends on the nature of the substituent groups at a benzene ring and the number of fluorine atoms. Thus, the IC_{50} values were 4.195 times higher for 4-fluoro, such as **8f**, and 688 times higher for compound **8g**, which contains 2,3-difluoro, compared to the standard drug lopinavir. On the other hand, compound **8h** containing 3-trifluoromethyl showed 1.853-fold decrease compared to lopinavir. Thus, the 3-trifluoromethyl side chain showed higher inhibition against SARS-CoV-3CL protease (IC_{50} = 240.6 μg/mL) than 4-fluoro (544.6 μg/mL) and 2,3-difluoro (868.2 μg/mL) as shown in Table 5 and Figure 8.

2.2.6. Molecular Docking Study. Additionally, compounds **8f−h** were docked with the active site of *N*-[(5-methylisoxazol-3-yl)carbonyl)alanyl-L-valyl-*N*1-((1*R*,2*Z*)-4-(benzyloxy)-4-oxo-1-{[(3*R*)-2-oxopyrolidin-3-yl]-methyl}but-2-enyl)-L-leucinamide (PDB ID: 6LU7). The binding modes of the ligand (PDB ID: 6LU7) with compounds **8f−h** were studied using molecular docking software 2015.10, and the results showed that the ligand formed four hydrogen bonds (HBs) with the

https://doi.org/10.1021/acsomega.3c01987
ACS Omega 2023, 8, 36636−36654

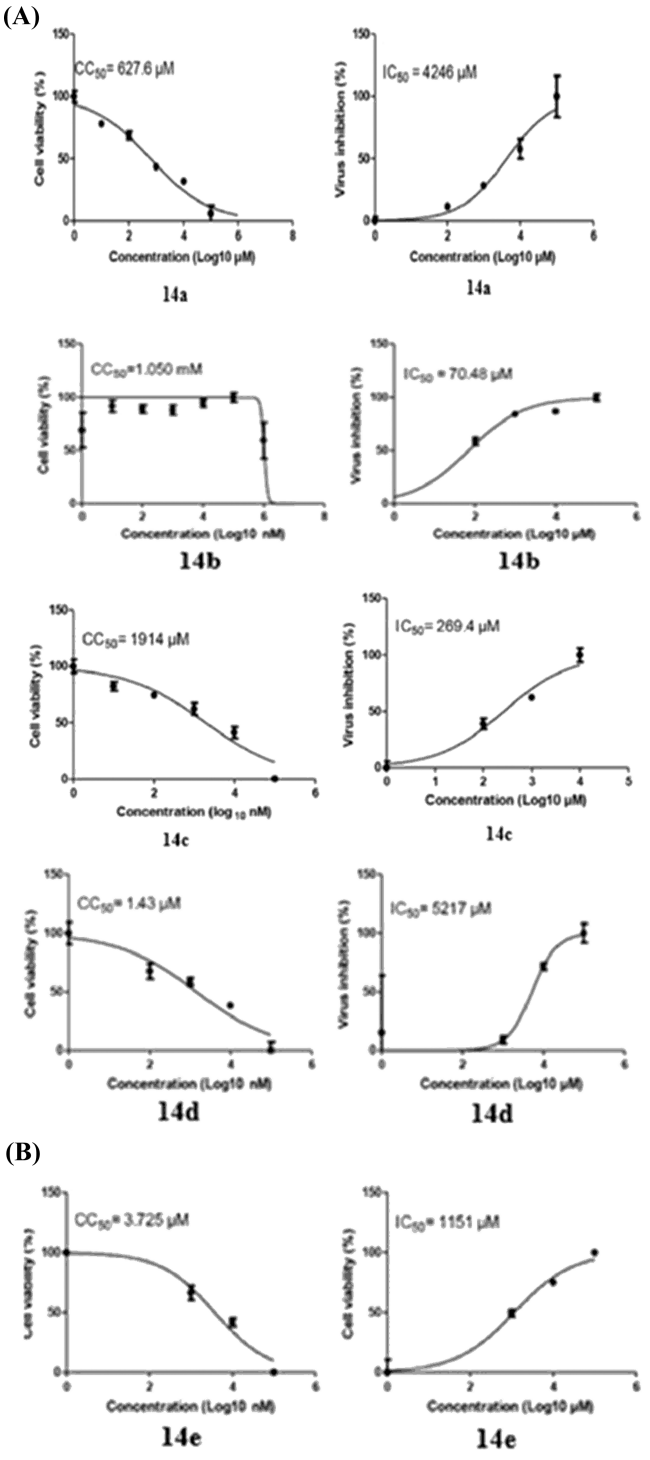

Figure 6. CC_{50} (50% cytotoxic concentration) of the tested *N*-pyridone-based triazoles in Vero-E6 cells and IC_{50} (50% inhibitory concentration) against NRC-03-nhCoV virus in Vero-E6 cells (A and B). CC_{50} and IC_{50} were plotted for each tested compound using Graph Pad Prism and were calculated from the nonlinear regression curve-fit analysis, relative to the virus and cell controls. Compound **14b** shows significant activity toward SARS-CoV-2 with IC_{50} = 70.48 μM and SI = 14.897 among the tested compounds **14a−e**.

active site of 6LU7 associated with a binding energy of −7.9074 kcal/mol and root-mean-square deviation (rmsd) equal to 1.6312; the first three HBs between the CO groups and Ans 142, Gly 143, and Glu 166 were with bond lengths of 3.08 3.2, and 3.18 Å, respectively. The interaction of HB between NH and Ans 143 had a bond length of 3.24 (Figures 9 and 10). The binding energy was −6.0086 kcal/mol, and the rmsd was 0.8430, indicating that compound **8f** fully occupied the receptor domains. Compound **8f** showed one hydrogen bond with a bond length of 3.22 Å between Gly 143 and the cyano group and another interaction between Glu 166 and arene-H of the thiophene ring (Figures 11 and 12). Compound **8g** showed two arene−H bond interactions of the benzothiophene moiety, His 163 and Glu 166 with a binding energy of −5.6918 kcal/mol and a rmsd of 0.7399 (Figures 13 and 14). Additionally, compound **8h**, which exhibited more potent anti-CoV-2 SARS activity, showed two hydrogen bond interactions with the active site of 6LU7, one between a cyano group and His 163 and the other between an amino group and Gln 189, with bond lengths of 3.09 and 3.10 Å associated with the bonging energy of −6.5953 kcal/mol and rmsd = 1.1970, in addition to another arene−H interaction between phenyl, which contains the trifluoromethyl group and Gly 143 (Figures 15 and 16). Furthermore, the standard drug lopinavir docked also with the active site 6LU7 with a binding energy of −7.1477 kcal/mol and rmsd equal to 1.0194. The results showed an HB interaction between Gln 189 and CO with a bond length of 3.03 Å, as well as two arene−phenyl interactions, the first an arene−arene interaction of His 41 and the second an arene-H with Pro 168 (Figures 17 and 18). These diverse binding modes of HBs formation affect the metabolism of the compounds, resulting in compounds **8a−h** being considered SARS-CoV-2 inhibitors.

3. CONCLUSIONS

In this study, a novel series of benzothiazolyl-pyridine hybrids were synthesized. The antiviral activity of these compounds was screened against H5N1, SARS-COV-2, and SARS-COV-2 viruses. The results showed that some of the synthesized compounds exhibited significant cytotoxic activity. Compounds **8f**, **8g**, and **14d** showed high antiviral effects against H5N1. Compounds **8f**, **8g** and **8h**, which contain fluoro groups, showed a good antiviral effect against SARS-COV-2. Furthermore, compound **8h**, with a 3-trifluoromethyl side chain, showed higher SARS-CoV-3CL protease inhibition (IC_{50} = 240.6 μg/mL) than 4-fluoro (544.6 μg/mL) and 2,3-difluoro (868.2 μg/mL) compared to lopinavir. These outcomes suggest that these compounds could be hopeful leads for producing more potent H1N5 and SARS-COV-2 inhibitors.

4. EXPERIMENTAL SECTION

4.1. Chemistry. All melting points were determined without correction using an Electrothermal (9100) apparatus. At Ain Shams, the ^{1}H and ^{13}C NMR spectra were recorded on a Bruker Avance (III)-400 Spectrometer (400 and 100 MHz, respectively) in DMSO-d_6 by using Si(Me)$_4$. At 70 eV, mass spectra were collected on a Shimadzu GCMS-QP 1000 Ex mass spectrometer and were achieved at Cairo University's Microanalyses Center. The IR spectra were done at Cairo University's Microanalyses Center as KBr pellets on a PerkinElmer 1430 spectrophotometer. Elemental analyses were carried out at Cairo University's Microanalyses Center using a Vario EL III Elemental CHNS analyzer. Biological evaluations of H5N1 and SARS-CoV-2 and mechanism of action of the newly synthesized compounds were performed at

https://doi.org/10.1021/acsomega.3c01987
ACS Omega 2023, 8, 36636−36654

Table 3. Anti-SARS-CoV-2 Activities of Compounds 14a−e

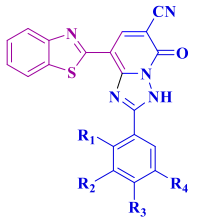

14a-e

compound no.	R_1	R_2	R_3	R_4	[a]CC_{50} (Vero-E6) μM	[b]IC_{50} (NRC-03-nhCoV) μM	[c]SI
14a	OMe	H	H	H	6276	4246	1.4781
14b	OMe	H	H	OMe	1050	70.48	14.897
14c	H	H	NH_2	H	1914	269.4	7.104
14d	H	H	$N(Me)_2$	H	143	5217	0.0274
14e	Cl	H	NO_2	H	3725	1151	3.236

[a]CC_{50}. [b]IC_{50} values were derived from results of at least two independent experiments in Vero cells infected with SARS-CoV-2. [c]SI (Selective index) = CC_{50}/IC_{50} for inhibitory SARS-CoV-2 infection.

Table 4. Mechanism of Action of Compounds 8f−h (Viral Titers)

compd no	conc (μM)	adsorption (PFU/mL)	viral inhibition (%)	viral replication (PFU/mL)	viral inhibition (%)	virucidal (PFU/mL)	viral inhibition (%)
8f	10	1×10^5	28.6	0.5×10^5	8.3	0.36×10^5	48
	1	1.2×10^5	26.5	0.5×10^5	0	0.32×10^5	40
	0.1	1.28×10^5	14.3	0.6×10^5	0	0.38×10^5	24
8g	10	1.0×10^5	33.3	0.6×10^5	60	0.3×10^5	80
	1	1.2×10^5	20	0.6×10^5	60	0.35×10^5	76.7
	0.1	1.4×10^5	7	0.7×10^5	53.3	0.4×10^5	73.3
8h	10	1.2×10^5	20	0.75×10^5	50	0.25×10^5	83.3
	1	1.2×10^5	20	0.85×10^5	43.3	0.3×10^5	80
	0.1	1.5×10^5	0	1.0×10^5	33.3	0.4×10^5	73.3
virus control		1.5×10^5		1.5×10^5		1.5×10^5	

the Center of Scientific Excellence for Influenza Viruses, Environmental Research Division, National Research Center (NRC), Dokki, and Cairo 12622, Egypt.

4.1.1. Synthesis of 2-Cyanomethylbenzothiazole ***3****.* At room temperature for 30 min, a mixture of *o*-aminothiophenol **1** (0.01 mol) and malononitrile **2** (0.01) was ground in a mortar with lemon juice (1 mL). The resulting solid was triturated with water, filtered, and recrystallized from methanol to yield pale yellow crystals **3**, yield 87%; mp 100 °C,[55] ν_{max}/cm^{-1} (KBr) 2225 (CN); ^{1}H NMR (DMSO-d_6) δ = 3.67 (s, 2H, CH_2), 7.51−7.53 (m, 2H, Ar), 8.02 (d, 1H, Ar), 8.18 (d, 1H, Ar); anal. calcd for $C_9H_6N_2S$: C, 62.05; H, 3.47; N, 16.08; S, 18.40. Found: C, 62.22; H, 3.67; N, 16.31; S, 18.21%.

4.1.2. Synthesis of 2-(Benzothiazolyl)-3-(dimethylamino)-acrylonitrile ***4****.* For 10 min, equimolar quantities of 2-cyanomethylbenzothiazole **3** and *N*,*N*-dimethylformamide dimethyl acetal (DMF-DMA) were ground in a mortar. The solid was triturated with water and recrystallized from ethanol to produce orange crystals with a melting point of 168 °C[56] and a 70% yield; ν_{max}/cm^{-1} (KBr) 2220 (CN); ^{1}H NMR (DMSO-d_6) δ = 3.0 (s, 3H, CH_3), 3.4 (s, 3H, CH_3), 7.38−7.75 (m, 4H, Ar), 7.76 (s, 1H, CH); anal. calcd for $C_{12}H_{11}N_3S$: C, 62.86; H, 4.84; N, 18.33; S, 13.98. Found: C, 62.65; H, 4.63; N, 18.56; S, 13.80%.

4.1.3. Synthesis of Compounds ***8a−h****.* In a mortar, equimolar amounts of compound **4** (0.01 mol) and *N*-aryl-2-cyanoacetamides **5a−h** (0.01 mol) were mixed for 20 min at room temperature in the presence of potassium hydroxide (0.01 mol). The resulting solid was triturated with water, purified, and then recrystallized from DMF to yield the products.

*4.1.3.1. 5-(Benzothiazolyl)-6-amino-1-(4-methoxyphenyl)-2-oxo-1,2-dihydropyridine-3-carbonitrile (****8a****).* Yellow crystals, yield 81%; mp 280 °C, ν_{max}/cm^{-1} (KBr) 3372 (NH_2) 2206 (CN), 1667 (CO); ^{1}H NMR (DMSO-d_6) δ = 3.85 (s, 3H, OCH_3), 7.16−7.50 (m, 6H, NH_2 and Ar); 7.85 (d, 2H, *J* = 8.8 Hz, Ar), 8.06 (d, 2H, *J* = 8.8 Hz, Ar), 8.40 (s, 1H, CH); ^{13}C NMR (DMSO-d_6) δ = 55.9, 116.11 117.9, 121.7, 122.2, 125.4, 126.8, 127.1, 130.2, 132.1, 144.6, 152.4, 155.0, 160.0, 160.4, 166.51; *m*/*z* = 374 (M^+, 100%), 359 (26.3%), 330 (5.8%), 252 (10.6%), 224 (12.8%), 197 (8.8%), 187 (6.8%), 123 (9.2%), 108 (27.0%), 77 (12.6%), 64 (10.4%); anal. calcd for $C_{20}H_{14}N_4O_2S$: C, 64.16; H, 3.77; N, 14.96; S, 8.56. Found: C, 64.34; H, 3.58; N, 14.74; S, 8.76%.

*4.1.3.2. 5-(Benzothiazolyl)-6-amino-1-(2,4-dimethoxyphenyl)-2-oxo-1,2-dihydro-pyridine-3-carbonitrile (****8b****).* Orange crystals, yield 79%; mp 288 °C, ν_{max}/cm^{-1} (KBr) 3398 (NH_2), 2195 (CN), 1640 (CO); ^{1}H NMR (DMSO-d_6) δ = 3.75 (s, 3H, OCH_3), 3.86 (s, 3H, OCH_3), 6.50−6.64 (m, 1H, Ar), 7.15−7.18 (m, 3H, Ar and NH_2), 7.32−7.36 (m, 1H, Ar), 7.66 (d, 1H, *J* = 7.2 Hz, Ar), 7.83 (d, 1H, *J* = 8.4 Hz, Ar), 8.05 (s, 1H, Ar), 8.11 (d, 1H, *J* = 7.2 Hz, Ar), 8.27 (s, 1H, CH); ^{13}C NMR (DMSO-d_6) δ = 55.7, 56.5, 74.8, 76.8, 99.1, 104.6, 120.1, 120.3, 120.5, 121.7, 122.9, 126.3, 144.4, 149.5, 155.0, 161.0, 165.0; *m*/*z* = 404 (M^+, 100%), 387 (11.5%), 373 (70.0%), 333 (31.5%), 251 (4.4%), 224 (16.3%), 198 (15.6%), 138 (18.8%), 122 (23.8%), 95 (31.4%), 77 (39.7%), 69 (58.1%), 56 (96.1%); anal. calcd for $C_{21}H_{16}N_4O_3S$: C, 62.36;

https://doi.org/10.1021/acsomega.3c01987
ACS Omega 2023, 8, 36636−36654

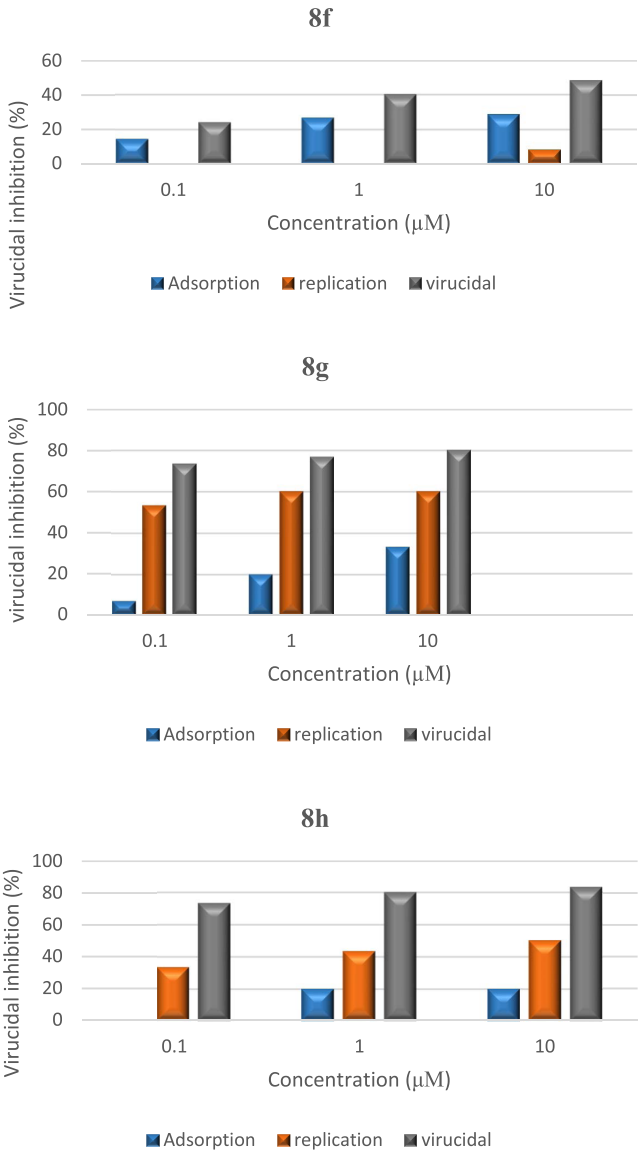

Figure 7. Modes of action of compounds **8f–h**. Viral Adsorption, replication, and virucidal mechanisms were studied for each compound at different concentrations using a plaque reduction assay. The three tested compounds act by the virucidal activity against SARS-CoV-2. The untreated virus was included in each mode of action for each compound as a virus control, and viral inhibition % for each mechanism for each tested compound calculated based on the percentage of virus reduction.

H, 3.99; N, 13.85; S, 7.93. Found: C, 62.55; H, 3.81; N, 13.62; S, 7.76%.

*4.1.3.3. 5-(Benzothiazolyl)-6-amino-1-(4-chloro-2-methylphenyl)-2-oxo-1,2-dihydro-pyridine-3-carbonitrile (**8c**).* Yellow crystals, yield 86%; mp 292 °C, ν_{max}/cm^{-1} (KBr) 3370 (NH_2), 2208 (CN), 1666 (CO); ^1H NMR (DMSO-d_6) δ = 2.06 (s, 3H, CH_3), 7.39–7.53 (m, 6H, Ar and NH_2), 7.64 (s, 1H, Ar), 7.90 (d, 1H, J = 4.4 Hz, Ar), 8.0 (d, 1H, J = 6 Hz, Ar), 8.49 (s, 1H, CH); m/z 392 = (M^+, 100%), 393 (M^+ + 1, 34.2%), 375 (81.2%), 340 (15.0%), 312 (15.1%), 223 (12.0%), 197 (22.9%), 164 (10.4%), 125 (14.4%), 109 (18.2%), 89 (45.0%), 77 (29.8%), 63 (30.3%), 51 (17.6%); anal. calcd for $C_{20}H_{13}ClN_4OS$: C, 61.15; H, 3.34; Cl, 9.02; N, 14.26; S, 8.16. Found: C, 61.32; H, 3.17; N, 14.49; S, 8.35%.

*4.1.3.4. 5-(Benzothiazolyl)-6-amino-1-(2,4-dichlorophenyl)-2-oxo-1,2-dihydropyridine-3-carbonitrile (**8d**).* Orange crystals, yield 92%; mp ≥ 300 °C, ν_{max}/cm^{-1} (KBr) 3378 (NH_2), 2196 (CN), 1644 (CO); ^1H NMR (DMSO-d_6) δ = 7.18–7.22 (m, 1H, Ar), 7.34–7.42 (m, 3H, Ar and NH_2), 7.65 (s, 1H, Ar), 7.69 (d, 1H, J = 6 Hz, 1H, Ar), 7.87 (d, 1H, J = 6.8 Hz, Ar), 8.26–8.28 (m, 2H, Ar), 8.35 (s, 1H, CH); ^{13}C NMR (DMSO-d_6) δ = 74.10, 78.50, 120.6, 121.8, 123.2, 124.2, 126.4, 127.3, 128.2, 128.9, 133.2, 135.4, 144.5, 154.6, 164.2; m/z = 412 (M^+, 48.5%), 413 (M^+ + 1, 15%), 414 (M^+ + 2, 31.6%), 392 (35.4%), 377 (69.4%), 224 (15.7%), 198 (15.1%), 124 (19.2%), 109 (36.1%), 97 (34.3%), 71 (45.9%), 69 (92.6%), 55 (100%); anal. calcd for $C_{19}H_{10}Cl_2N_4OS$: C, 55.22; H, 2.44; Cl, 17.16; N, 13.56; S, 7.76. Found: C, 55.42; H, 2.61; N, 13.79; S, 7.94%.

*4.1.3.5. 5-(Benzothiazolyl)-6-amino-1-(4-bromophenyl)-2-oxo-1,2-dihydropyridine-3-carbonitrile (**8e**).* Beige crystals, yield 79%; mp ≥ 300 °C, ν_{max}/cm^{-1} (KBr) 3327 (NH_2), 2211 (CN), 1652 (CO); ^1H NMR (DMSO-d_6) δ = 7.19 (d, 1H, J = 7.6 Hz, Ar); 7.28 (d, 1H, J = 7.6 Hz, Ar); 7.38–7.69 (m, 8H, Ar and NH_2), 8.39 (s, 1H, CH); anal. calcd for $C_{19}H_{11}BrN_4OS$: C, 53.91; H, 2.62; Br, 18.88; N, 13.24; S, 7.57. Found: C, 53.72; H, 2.83; N, 13.47; S, 7.39%.

*4.1.3.6. 5-(Benzothiazolyl)-6-amino-1-(4-fluorophenyl)-2-oxo-1,2-dihydropyridine-3-carbonitrile (**8f**).* Beige crystals, yield 75%; mp ≥ 300 °C, ν_{max}/cm^{-1} (KBr) 3356 (NH_2), 2208 (CN), 1666 (CO); ^1H NMR (DMSO-d_6) δ = 7.28–7.48 (m, 6H, Ar and NH_2); 7.87 (d, 1H, J = 7.6 Hz, Ar); 8.02–8.04 (m, 2H, Ar), 8.06 (d, 1H, J = 8 Hz, Ar), 8.43 (s, 1H, CH); m/z 362 = (M^+, 100%), 318 (7.3%), 197 (8.8%), 146 (5.5%), 111 (18.0%), 95 (35.9%), 75 (20.5%), 69 (22.9%), 55 (6.7%); anal. calcd for $C_{19}H_{11}FN_4OS$: C, 62.97; H, 3.06; F, 5.24; N, 15.46; S, 8.85. Found: C, 62.77; H, 3.25; N, 15.21; S, 8.67%.

*4.1.3.7. 5-(Benzothiazolyl)-6-amino-1-(2,3-difluorophenyl)-2-oxo-1,2-dihydropyridine-3-carbonitrile (**8g**).* Beige crystals, yield 71%; mp = 286 °C, ν_{max}/cm^{-1} (KBr) 3433 (NH_2), 2212 (CN), 1641 (CO); ^1H NMR (DMSO-d_6) δ = 7.26–7.46 (m, 7H, Ar and NH_2); 7.86 (d, 1H, J = 7.8 Hz, Ar); 8.02 (d, 1H, J = 7.8 Hz, Ar), 8.41 (s, 1H, CH); ^{13}C NMR (DMSO-d_6) δ = 80.5, 100.4, 119.9, 121.0, 121.4, 121.7, 123.3, 125.8, 126.5, 134.3, 134.7, 151.3, 152.5, 156.8, 160.3, 162.6, 165.6; m/z 380 = (M^+, 100%), 360 (50.7%), 332 (26.4%), 224 (9.2%), 197 (11.3%), 170 (6.76%), 146 (7.28%), 129 (12.16), 113 (18.29%), 96 (5.1%), 69 (23.3%); anal. calcd for $C_{19}H_{10}F_2N_4OS$: C, 60.0; H, 2.65; F, 9.99; N, 14.73; S, 8.43. Found: C, 60.19; H, 2.83; N, 14.49; S, 8.61%.

*4.1.3.8. 5-(Benzothiazolyl)-6-amino-1-[3-(trifluoromethyl)phenyl]-2-oxo-1,2-dihydro-pyridine-3-carbonitrile (**8h**).* Beige crystals, yield 78%; mp ≥ 300 °C, ν_{max}/cm^{-1} (KBr) 3428 (NH_2), 2213 (CN), 1643 (CO); ^1H NMR (DMSO-d_6) δ = 7.27–7.31 (m, 4H, Ar); 7.41 (m, 2H, Ar); 7.86 (d, 2H, J = 8.1 Hz, Ar); 8.02 (d, 2H, J = 7.8 Hz, Ar); 8.41 (s, 1H, CH); ^{13}C NMR (DMSO-d_6) δ = 80.5, 100.4, 120.0, 121.0, 121.7, 123.3, 125.9, 134.3, 134.7, 152.1, 152.5, 156.9, 161.0, 162.6, 165.6; anal. calcd for $C_{20}H_{11}F_3N_4OS$: C, 58.25; H, 2.69; F, 13.82; N, 13.59; S, 7.77. Found: C, 58.43; H, 2.50; N, 13.82; S, 7.94%.

*4.1.4. Synthesis of Compounds **14a–e**.* Equimolar amounts of **4** (0.01 mol) and 2-cyano-*N*′-(4-substituted benzylidene) acetohydrazide **9a–e** (0.01 mol) were ground in a mortar in the presence of potassium hydroxide for 20 min at room temperature. The solid so formed was triturated with water, filtered off, and then recrystallized from DMF.

https://doi.org/10.1021/acsomega.3c01987
ACS Omega 2023, 8, 36636–36654

Table 5. Resulting Data of IC_{50} of Compounds 8f–h and a Lopinavir against CoV-3CL Protease

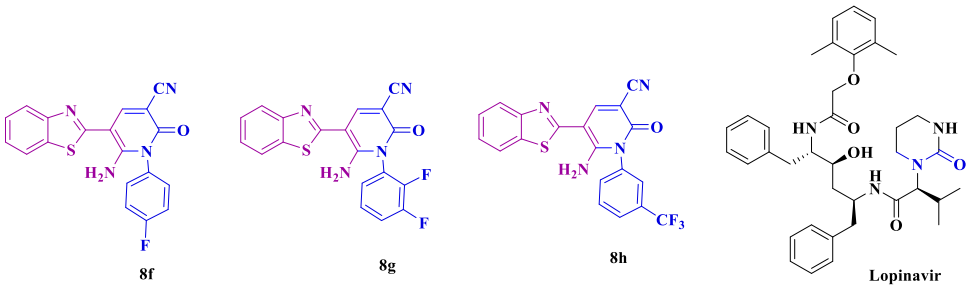

compound no.	IC_{50} (μg/mL)	SD±
8f	544.6	27.6
8g	868.2	44
8h	240.6	12.2
lopinavir	129.8	6.58

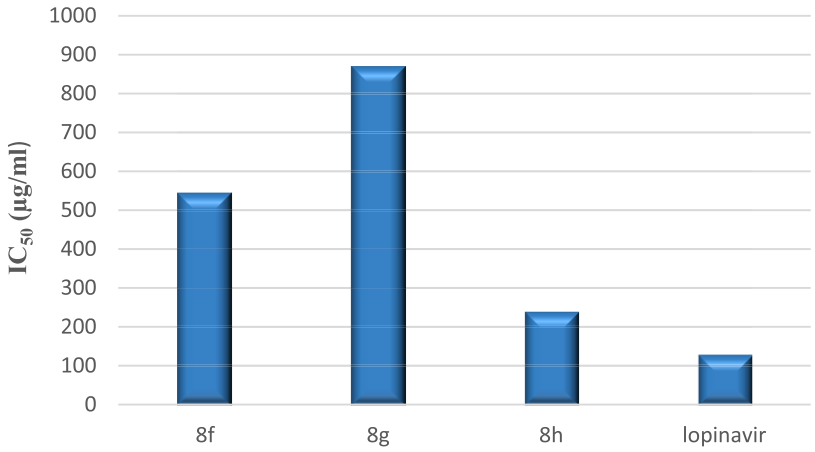

Figure 8. IC_{50} graph of compounds **8f–h** against CoV-3CL protease and Lopinavir.

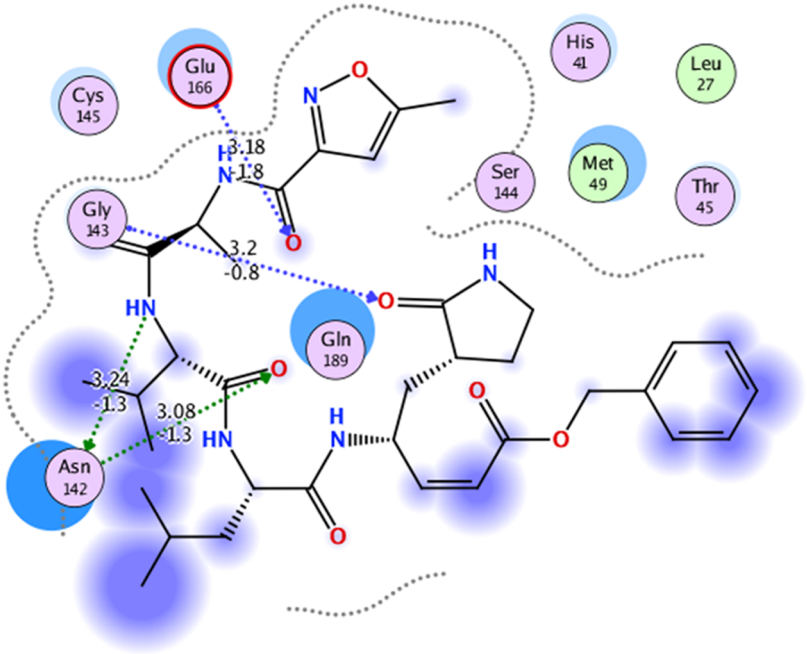

Figure 9. Interaction in 2D of the active site of 6LU7.

4.1.4.1. 8-(Benzothiazolyl)-2-(2-methoxyphenyl)-5-oxo-3,5-dihydro[1,2,4]triazolo[1,5- a]-pyridine-6-carbonitrile ***(14a)***. Reddish brown crystals, yield 74%; mp ≥ 300 °C, ν_{max}/cm^{-1} (KBr) 3431 (NH), 2195 (CN), 1609 (CO); ^1H

https://doi.org/10.1021/acsomega.3c01987
ACS Omega 2023, 8, 36636–36654

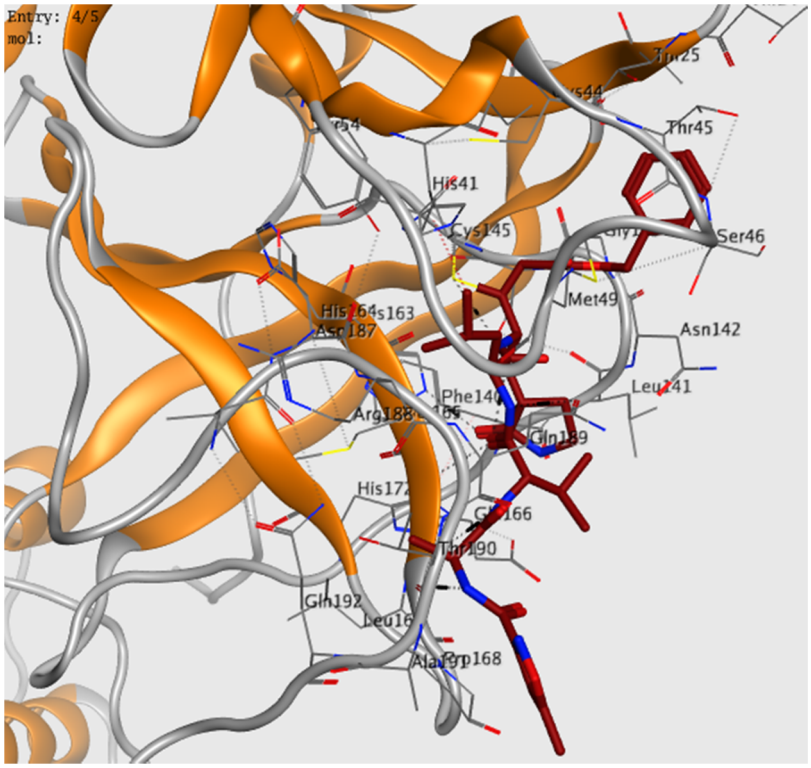

Figure 10. Interaction in 3D of the ligand active site of 6LU7 (in yellow color).

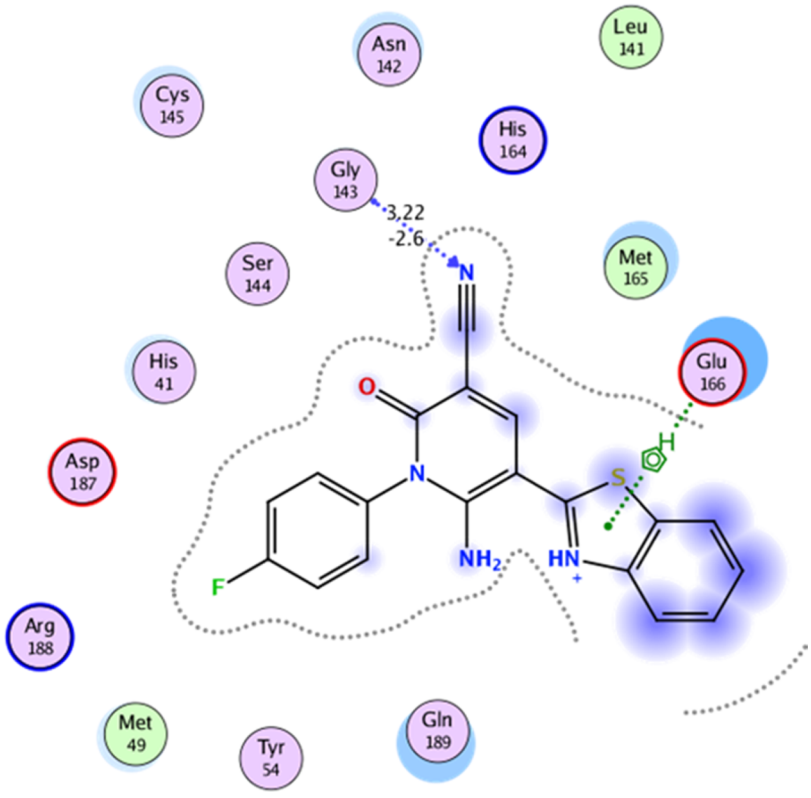

Figure 11. Interaction in 2D of compound **8f** with an active site of 6LU7.

NMR (DMSO-d_6) δ = 3.88 (s, 3H, OCH_3), 7.12 (t, 1H, J = 7.2 Hz, Ar), 7.32 (t, 1H, J = 7.6 Hz, Ar), 7.44−7.52 (m, 2H, Ar), 7.74 (d, 1H, J = 7.8 Hz, Ar), 7.90 (d, 1H, J = 8 Hz, Ar), 8.03 (m, 3H, Ar and NH), 8.47 (s, 1H, CH); ^{13}C NMR (DMSO-d_6) δ = 56.3, 81.1, 101.11, 112.8, 117.7, 120.7, 121.5, 122.2, 123.8, 126.3, 131.4, 131.7, 134.9, 135.2, 152.0, 153.0, 157.5, 158.1, 160.5, 161.1; anal. calcd for $C_{21}H_{13}N_5O_2S$: C, 63.15; H,

https://doi.org/10.1021/acsomega.3c01987
ACS Omega 2023, 8, 36636−36654

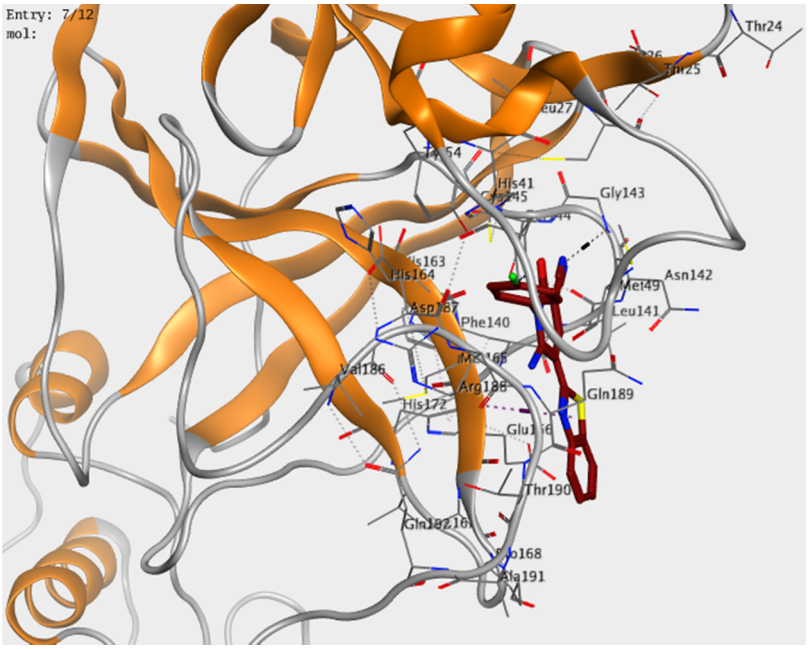

Figure 12. Interaction in 3D of compound **8f** (in brown color) with the active site of 6LU7.

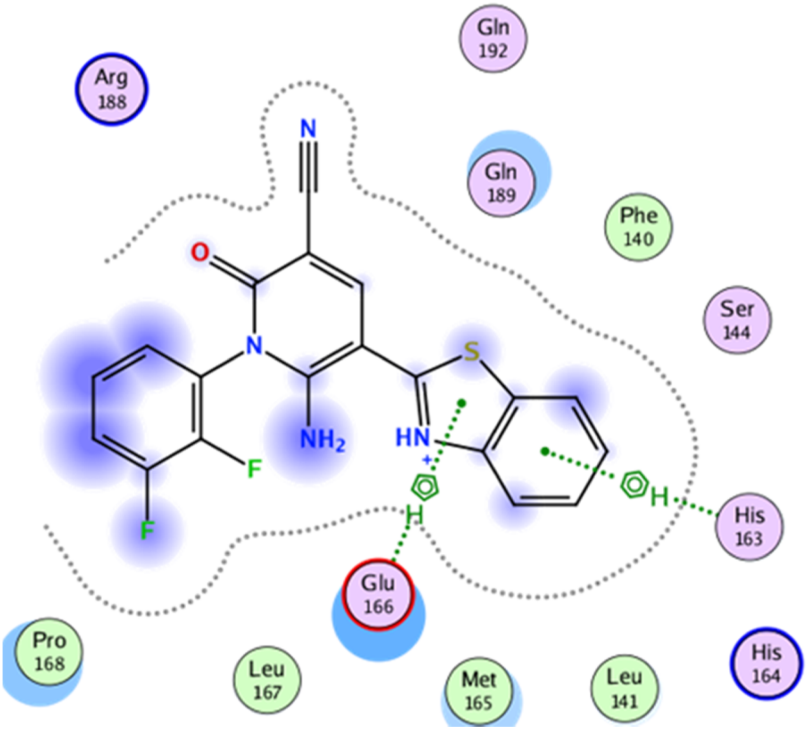

Figure 13. Interaction in 2D of compound **8g** with the active site of 6LU7.

3.28; N, 17.53; S, 8.03. Found: C, 63.34; H, 3.45; N, 17.75; S, 8.20%.

*4.1.4.2. 8-(Benzothiazolyl)-2-(2,5-dimethoxyphenyl)-5-oxo-3,5-dihydro[1,2,4]triazolo[1,5-a]-pyridine-6-carbonitrile (**14b**).* Reddish brown crystals, yield 83%; mp ≥ 300 °C, ν_{max}/cm^{-1} (KBr) 3398 (NH), 2206 (CN), 1612 (CO); ^{1}H NMR (DMSO-d_6) δ = 3.85 (s, 3H, OCH_3), 3.91 (s, 3H, OCH_3), 7.06−7.15 (m, 2H, Ar), 7.30−7.44 (m, 3H, Ar and NH), 7.56 (s, 1H, Ar), 7.90 (d, 1H, J = 7.6 Hz, Ar), 8.07 (d, 1H, J = 7.6 Hz, Ar), 8.47 (s, 1H, CH); ^{13}C NMR (DMSO-d_6) δ = 56.0, 57.2, 81.1, 101.1, 114.7, 116.6, 117.1, 120.4, 121.5, 121.8, 122.2, 123.8, 126.3, 135.0, 135.2, 152.1, 152.9, 153.4, 160.3, 163.0; anal. calcd for $C_{22}H_{15}N_5O_3S$: C, 61.53; H, 3.52; N, 16.31; S, 7.47. Found: C, 61.71; H, 3.69; N, 16.09; S, 7.29%.

*4.1.4.3. 8-(Benzothiazolyl)-2-(4-aminophenyl)-5-oxo-3,5-dihydro[1,2,4]triazolo[1,5-a]-pyridine-6-carbonitrile (**14c**).* Dark brown crystals, yield 84%; mp ≥ 300 °C, ν_{max}/cm^{-1} (KBr) 3345 (NH_2), 3220 (NH), 2203 (CN), 1617 (CO); ^{1}H NMR (DMSO-d_6) δ = 6.71 (s, 2H, NH_2), 7.19−7.89 (m, 7H, Ar and NH), 7.97 (d, 2H, J = 8.4 Hz, Ar), 8.46 (s, 1H, CH); m/z = 384 (M^+, 3.7%), 358 (15%), 305 (3.4%), 251 (5.8%), 223 (7.03%), 185 (3.7%), 146 (6.4%), 135 (25.49%), 106

https://doi.org/10.1021/acsomega.3c01987
ACS Omega 2023, 8, 36636−36654

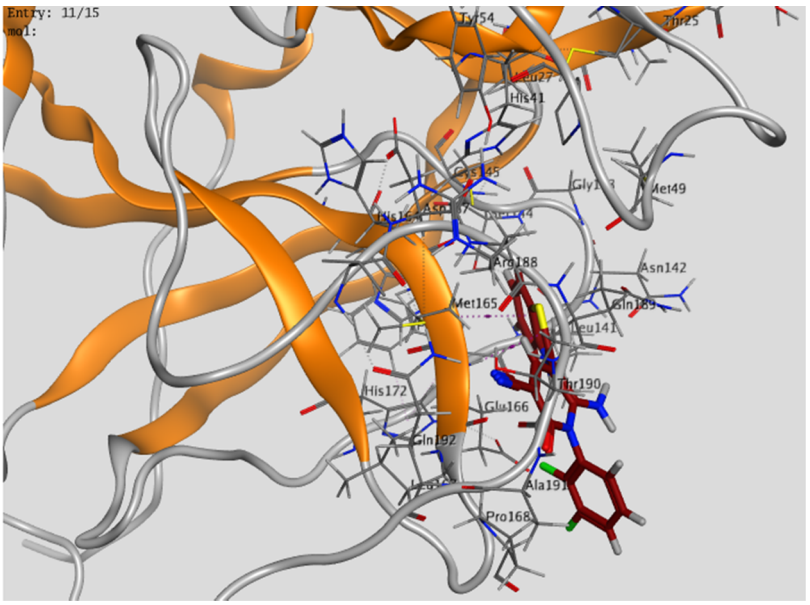

Figure 14. Interaction in 3D of compound **8g** (in brown color) with an active site of 6LU7.

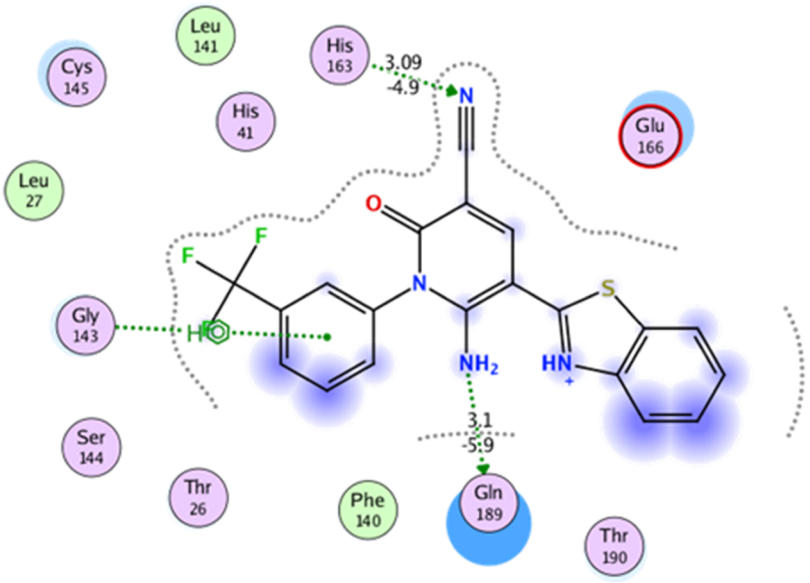

Figure 15. Interaction in 2D of compound **8h** with an active site of 6LU7.

(28.7%) 85 (32.1%) 55 (100%); anal. calcd for $C_{20}H_{12}N_6OS$: C, 62.49; H, 3.15; N, 21.86; S, 8.34. Found: C, 62.31; H, 3.34; N, 21.63; S, 8.17%.

*4.1.4.4. 8-(Benzothiazolyl)-2-(4-(dimethylamino)phenyl)-5-oxo-3,5-dihydro[1,2,4]- triazolo[1,5-a]pyridine-6-carbonitrile (**14d**).* Black crystals, yield 71%; mp ≥ 300 °C, ν_{max}/cm^{-1} (KBr) 3384 (NH), 2195 (CN), 1605 (CO); ^{1}H NMR (DMSO-d_6) δ = 2.99 (s, 6H, CH_3), 6.85 (d, 1H, J = 8.8 Hz, Ar), 7.30 (t, 1H, J = 7.6 Hz, Ar), 7.44 (t, 1H, J = 8 Hz, Ar), 8.08−8.12 (m, 5H, Ar and NH), 8.15 (d, 1H, J = 8.4 Hz, Ar), 8.45 (s, 1H, CH); ^{13}C NMR (DMSO-d_6) δ = 66.8, 81.2, 112.2, 121.4, 122.2, 123.8, 128.4, 151.8, 153.0, 158.7, 161.4; m/z 412 = (M^+, 3.4%), 381 (4.5%), 305 (92.4%), 279 (16.6%), 223 (3.5%), 185 (4.09%), 149 (16.1%), 132 (34.08%), 97 (28.2%), 73 (54.3%), 69 (71.3%), 57 (100%), 55 (87.5%); anal. calcd for $C_{22}H_{16}N_6OS$: C, 64.06; H, 3.91; N, 20.38; S, 7.77. Found: C, 64.25; H, 3.73; N, 20.60; S, 7.59%.

*4.1.4.5. 8-(Benzothiazolyl)-2-(2-chloro-4-nitrophenyl)-5-oxo-3,5-dihydro[1,2,4]triazolo1,5-a]pyridine-6-carbonitrile (**14e**).* Reddish brown crystals, yield 76%; mp ≥ 300 °C, ν_{max}/cm^{-1} (KBr) 3398 (NH), 2206 (CN), 1612 (CO); ^{1}H NMR (DMSO-d_6) δ = 6.80−7.35 (m, 3H, Ar), 7.45 (d, 1H, J = 8 Hz, Ar), 7.51−7.60 (m, 3H, Ar and NH), 8.15 (d, 1H, J = 8.4 Hz, Ar), 8.50 (s, 1H, CH); ^{13}C NMR (DMSO-d_6) δ = 95.2, 102.4, 117.7, 119.6, 120.9, 122.8, 123.9, 125.8, 127.6, 128.8, 132.9, 137.0, 152.5, 156.9, 158.5, 159.9, 161.8; anal. calcd for $C_{20}H_9ClN_6O_3S$: C, 53.52; H, 2.02; Cl, 7.90; N, 18.72; S, 7.14. Found: C, 53.70; H, 2.19; N, 18.49; S, 7.35%.

4.2. Biological Section. *4.2.1. Virus, cell, and MTT assay.* At 37 °C, 5% CO_2, the virus and Vero-E6 cells were grown in Dulbecco's Modified Eagle's medium (DMEM) containing 10% FBS (Invitrogen) and 1% pen/strep antibiotic mixture. To yield virus stock, cells were distributed in tissue culture jars for 24 h before infection with CoV-19/Egypt/NRC-3/2020

https://doi.org/10.1021/acsomega.3c01987
ACS Omega 2023, 8, 36636−36654

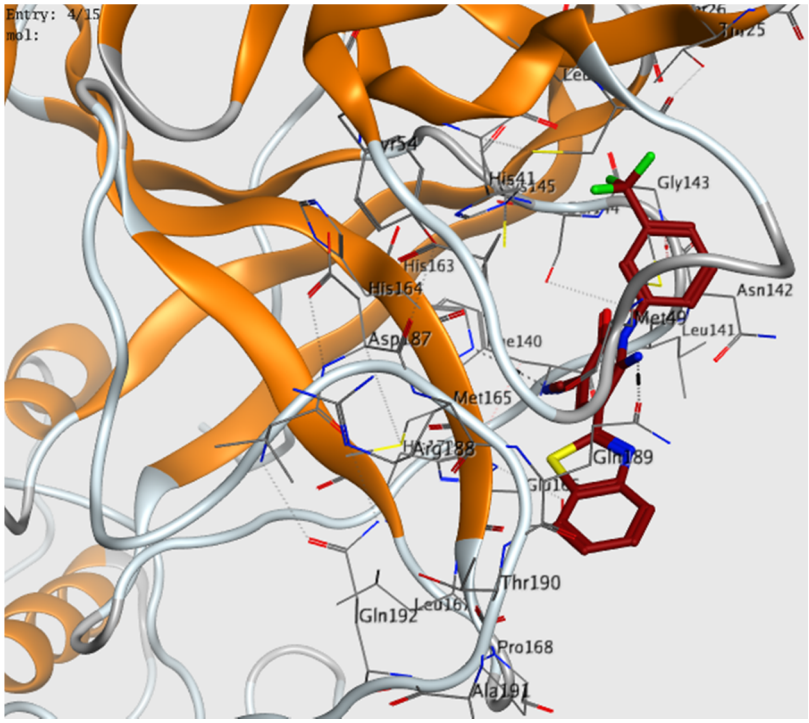

Figure 16. Interaction in 3D of compound **8h** (in brown color) with the active site of 6LU7.

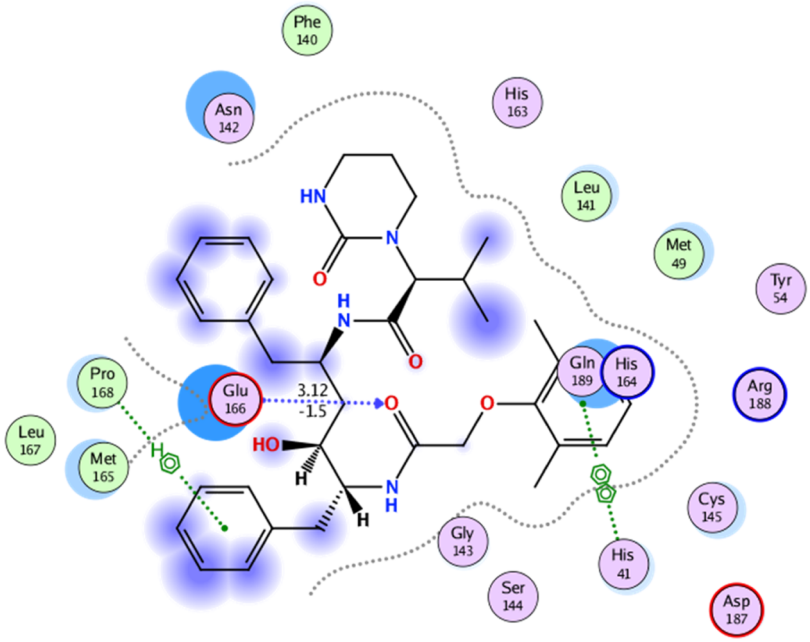

Figure 17. Interaction in 2D of lopinavir with the active site of 6LU7.

isolates at a multiplicity of infection (MOI) of 0.1 infection medium (DMEM containing 2% FBS, 1% pen/strep, and 1% TPCK-treated trypsin). The infection medium comprising of the virus inoculum was enlarged 2 h later. To produce virus stock, cells were dispersed into tissue culture jars for 24 h earlier to infection with CoV-19/Egypt/NRC-3/2020 isolate at a MOI of 0.1 infection medium (DMEM including 2% FBS, 1% pen/strep, and 1% TPCK-treated trypsin). The virus inoculum-containing infection medium was ejected 2 h later and replaced with a fresh infection medium, incubated for 3 days. Cell supernatant was collected at the indicated time point and centrifuged for 5 min at 2500 rpm to remove small particulate cell flotsam and jetsam. The supernatant was transferred to a new 50 mL falcon tube, and the plaque infectivity assay was used to titrate it.

The following steps carried out the method.

I. Stock solutions of the test compounds were prepared in 10% DMSO in DDH_2O and diluted further to working solutions with DMEM to determine the half-maximal cytotoxic concentration (CC_{50}). The extracts' cytotoxic activity was determined in Vero-E6 cells using the MTT process, which was slightly modified.

https://doi.org/10.1021/acsomega.3c01987
ACS Omega 2023, 8, 36636−36654

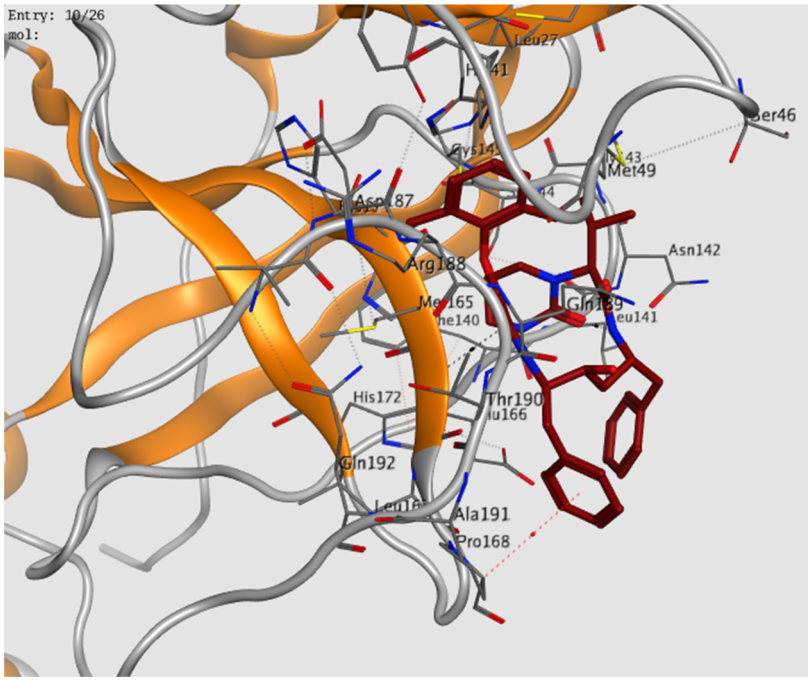

Figure 18. Interaction in 3D of lopinavir (in brown color) with the active site of 6LU7 (in yellow color).

II. The cells were seeded in 96-well plates (100 l/well at a density of 3105 cells/mL) and incubated at 37 °C in 5% CO_2 for 24 h. Cells were treated in triplicates with different concentrations of the studied compounds after 24 h.
III. The supernatant was discarded after 24 h, and cell monolayers were washed three times with phosphate-buffered saline (PBS). MTT solution (20 l of 5 mg/mL stock solution) was applied to each well and incubated at 37 °C for 4 h before medium aspiration.
IV. Formazan crystals were dissolved in each well with 200 mL of acidified isopropanol (0.04 M HCl in isopropanol).
V. Using a multiwell plate reader, the absorbance of formazan solutions was measured at max 540 nm with 620 nm as a reference wavelength.
VI. The following equation was used to calculate the percentage of cytotoxicity relative to untreated cells. The concentration that exhibited 50% cytotoxicity was calculated using a plot of percent cytotoxicity versus sample concentration.[63]

(Absorbance of cells without treatment − absorbance of cells with treatment) × 100 absorbance's cells without treatment = % cytotoxicity

4.2.2. Plaque Infectivity Assay. The plaque infectivity assay was used to titrate hCoV-19/Egypt/NRC-03/2020 (NRC-03-nhCoV) (Accession Number on GSAID: EPI-ISL-430820) as previously mentioned. In a nutshell, the propagated virus was serially diluted 10-fold in a medium containing no FBS. To inoculate 80−90% confluent Vero-E6 cell monolayers, 100 L of each virus dilution was combined with 400 L of infection medium and used to inoculate 80−90% confluent Vero-E6 cell monolayers.

A control well was inoculated with 500 mL of serum-free medium in the same plate, then incubated for 1 h at 37 °C with 5% CO_2 to enable virus adsorption and rocked every 15 min to ensure uniform infection and prevent drying of the cells. The virus inoculum was discarded after 1 h. The cell monolayers were overlaid with 3 mL of DMEM plus 0.6% agarose containing 1 g/mL TPCK-treated trypsin, 10% FBS, one pen/strep, and the required concentration of the test drug. The plate was left at R.T. for 10 min to enable the agarose portion of the overlayer medium to solidify before being incubated at 37 °C under 5% CO_2. After 72 h, 1 mL of fixation solution (10% formalin) was applied to each well for 1 h for cell fixation and virus inactivation. The fixer was eventually discarded, and the plate wells were washed and dried. One mL of the staining solution (0.1% crystal violet) was applied to each well for 5 min to visualize the plaques, then the dye was discarded, and the plate wells were rinsed in water. In a violet (stained cells) background, viral plaques appeared as simple unstained spots (due to viral infection). The following equation was used to measure the virus titer

Plaque-forming unit (PFU) per mL = number of plaques multiplied by the virus's inoculated volume multiplied by the virus's dilution factor of 10.[64]

4.2.3. Plaque Reduction Assay. The plaque reduction assay[65] was performed in a six-well plate with Vero-E6 cells (1.2 106 cells) cultivated for 24 h at 37 °C to determine the preliminary antiviral activity of the FDA-approved drugs. Before being applied to the cells, the NRC-03-nhCoV virus was diluted to give 102 plaque-forming units (PFU) per well, combined with the safe concentration of the tested compounds, and incubated for 1 h at 37 °C. The cells were inoculated with (100 mL/well) virus with the tested compounds after removing the growth medium from the cell culture plates. After 1 h of virus adsorption, the cell monolayers were given 3 mL of DMEM supplemented with the overlay medium containing specified concentrations of the tested compounds. The plates were allowed to solidify before incubating at 37 °C for 3 days to form viral plaques. After 1 h in cell fixing solution, the plates were stained with 0.1% crystal violet in distilled water. The untreated virus was incubated with Vero-E6 cells in control wells, and plaques were

https://doi.org/10.1021/acsomega.3c01987
ACS Omega 2023, 8, 36636−36654

counted, and the percentage reduction in plaque formation was calculated.

4.2.4. Inhibitory Concentration 50 (IC_{50}). Vero-E6 cells were distributed in each well of 96-well tissue culture plates and incubated overnight in a humidified 37 °C incubator under a 5% CO_2 environment. After that, the cell monolayers were washed in 1 PBS and exposed to virus adsorption for 1 h at room temperature. The monolayers were then overlaid with 50 μmol DMEM containing differing concentrations of the selected test compounds azithromycin, niclosamide, and nitazoxanide. The cells were fixed with 100 l of 4% paraformaldehyde for 20 min and stained with 0.1% crystal violet in distilled water for 15 min after being incubated at 37 °C in a 5% CO_2 incubator for 72 h. The optical density of the color was calculated at 570 nm using an Anthos Zenyth 200 rt plate reader after the crystal violet dye was dissolved in 100 mL of absolute methanol per well (Anthos Lab tec Instruments, Heerhugowaard, Netherlands). The compound's IC_{50} is described as the amount of the compound needed to reduce the virus-induced cytopathic effect (CPE) by 50% when compared to the virus control.[66]

To test the effect of different virus concentrations on replication performance, confluent Vero-E6 cell monolayers were infected in triplicate with NRC-03-nhCoV at MOIs of 0.005, 0.001, and 0.001 at 37 °C. At 1 h postinfection (hpi), the inocula were removed, the cell monolayers were washed with 1 PBS, and infection media (1 DMEM supplemented with 1% Pen/Strep, 0.3% bovine serum albumin (BSA), and 2 g/mL TPCK-treated trypsin) was overlaid. At 48 h post-induction, the cell culture supernatants were collected. A plaque infectivity assay was used to assess the virus titer.

4.2.5. Viral Adsorption Mechanism. Zhang et al.[67] used a procedure with minor changes to investigate the viral adsorption process. Vero-E6 cells were grown for 24 h at 37 °C in a 6-well plate (105 cells per mL). Each medication was mixed into 200 L of medium without supplements and incubated with the cells for 2 h at 4 °C. The nonabsorbed drug was extracted from the inocula by washing the cells three times with a supplement-free medium. The pretreated cells were coincubated for 1 h with SARS-CoV-2 virus diluted to 104 PFU/well, and then 3 mL of DMEM supplemented with 2% agarose was added. Plates were allowed to solidify before being incubated at 37 °C to allow viral plaques to form. The plaques were fixed and stained as mentioned above to measure the percentage reduction in plaque formation compared to the control wells, which contained untreated Vero-E6 cells directly infected with NRC-03-nhCoV.

4.3.6. Viral Replication Mechanism. As previously mentioned,[68] the effect of the tested drug on viral replication was determined, which Vero-E6 cells were grown for 24 h at 37 °C in a 6-well plate (105 cells per mL). The virus was inoculated directly into the cells and incubated at 37 °C for 1 h. Three times with a supplement-free medium, washing the cells removed the nonadsorbed viral particles from the inocula. Crystal violet was used to stain cell monolayers after being fixed in a 10% formalin solution for 1 h, then Vero-E6 cells were incubated with the virus in the control wells. The number of plaques formed was counted, and the percentage reduction in plaque formation was compared to that in control wells.

4.3.7. Virucidal Mechanism. The virucidal mechanism was investigated using a protocol previously mentioned[69] Vero-E6 cells (105 cells/mL) were grown for 24 h at 37 °C in a 6-well plate, and 200 mL of serum-free DMEM containing SARS-CoV-2 was added to each sample with promising inhibition. The mixture was diluted 10-fold three times in a serum-free medium after 1 h of incubation, and viral particles could still develop on Vero-E6 cells. The Vero-E6 cell monolayer was then treated with 100 mL of each dilution. After 1 h of contact time, a DMEM overlayer was added to the cell monolayer. Plates were allowed to solidify before being incubated at 37 °C to allow viral plaques to form. The plaques were fixed and stained to measure the percentage reduction in the level of plaque formation, as mentioned above. This value was compared to that of control wells that contained virus-infected cells that had not been pretreated with the tested substance.

4.2.8. Molecular Modeling. SARS-CoV-2 main protease (Mopar) (PDB ID: 6LU7) X-ray crystal structure coordinate was discovered using PDB. The MOE 2015.10 software was used to perform the docking study.

■ ASSOCIATED CONTENT

Supporting Information

The Supporting Information is available free of charge at https://pubs.acs.org/doi/10.1021/acsomega.3c01987.

Experimental details: chemistry, biological evaluations, MTT assay, molecular docking, characterization data of all compounds, ^{1}H NMR, ^{13}C NMR, IR, mass spectra, and IC_{50} for tested compounds (PDF)

■ AUTHOR INFORMATION

Corresponding Author

Nadia Hanafy Metwally − *Chemistry Department, Faculty of Science, Cairo University, Cairo 12613, Egypt;* orcid.org/0000-0002-9706-3694; Email: mnadia@sci.cu.edu.eg

Authors

Galal Hamza Elgemeie − *Chemistry Department, Faculty of Science, Helwan University, Cairo 11785, Egypt;* orcid.org/0000-0003-3268-5975

Fatma Gomaa Fahmy − *Chemistry Department, Faculty of Science, Cairo University, Cairo 12613, Egypt*

Complete contact information is available at: https://pubs.acs.org/10.1021/acsomega.3c01987

Notes

The authors declare no competing financial interest.

■ REFERENCES

(1) Cheung, T. K. W.; Pool, L. M. Biology of influenza a virus. *Ann. N. Y. Acad. Sci.* **2007**, *1102*, 1−25.

(2) Liu, Q.; Liu, D. Y.; yang, Z. Q. Characteristics of human infection with avian influenza viruses and development of new antiviral agents. *Acta Pharm. Sinica* **2013**, *34*, 1257−1269.

(3) World Health Organization. Cumulative number of confirmed human cases of Avian influenza A/(H5N1) reported to WHO. Http://www.who.int/csr/disease/avian_influenza/country/cases_table_2006_3_01/en/index.html.

(4) WHO. Cumulative number of confirmed cases for avian influenza A (H5N1) reported to WHO, 2003−2004. Epidemic Pandemic Alert Response World Heal Organ 1−3. 2020.

(5) Aledavood, E.; Selmi, B.; Estarellas, C. From acid activation mechanisms of proton conduction to design of inhibitors of the M2 proton channel of influenza A virus. *Front. Mol. Biosci.* **2022**, *8*, No. 796229.

(6) H Saffaei, A.; Aminoari, N. S.; Moorthy, N. S. H. N.; Poongavanam, V.; Pratheepa, V. Viral M2 ion channel protein: A

promising target for anti-influenza drug discovery. *Mini Rev. Med. Chem.* **2014**, *15* (14), 819−830.
(7) Swierczynska, M. S.; Guzel, D. M. M.; Pindelska, E. Antiviral drug in influenza. *Int. J. Environ. Res. Public Health* **2022**, *19*, 3018.
(8) Su, H. C.; Feng, I. J.; Tang, H. T.; Shih, M. F.; Hua, Y. M. Comparative effectiveness of neuraminidase inhibitors in patients with influenza: A systematic review and network meta-analysis. *J. Infect. Chemother.* **2022**, *28*, 158−169.
(9) Sahraei, Z.; Shabani, M.; Shokouhi, S.; Saffaei, A. Aminoquinolines against coronavirus disease 2019 (COVID-19): Chloroquine or hydroxychloroquine. *Int. J. Antimicrob. Agents* **2020**, *55*, No. 105945.
(10) Scuccimarri, R.; Sutton, E.; Fitzcharles, M. A. Hydroxychloroquine: A Potential ethical dilemma for rheumatologists during the COVID-19 pandemic. *J. Rheumatol.* **2020**, *47*, 783−786.
(11) Elfiky, A. A. Anti-HCV, nucleotide inhibitors, repurposing against COVID-19. *Life Sci.* **2020**, *248*, No. 117477.
(12) Deng, J.; Zhou, F.; Hou, W.; Heybati, K.; Ali, A.; Chang, O.; Silver, Z.; Dhivagaran, T.; Ramaraju, H. B.; Wong, C. Y.; Zuo, Q. K.; Lapshina, E.; Mellett, M. Efficacy of lopinavir-ritonavir combination therapy for the treatment of hospitalized COVID-19 patients: a meta-analysis. *Future Virol.* **2022**, *17*, 169−189.
(13) Gupta, M. K.; Venula, S.; Donde, R.; Gouda, G.; Behera, L.; Vadde, R. K. In silico approaches to detect inhibitors of the human severe acute respiratory syndrome coronavirus envelope protein ion channel. *Biomol. Struct. Dyn.* **2021**, *39*, 2617−2627.
(14) Montaño, L.; Sommer, B.; Verjan, J. C. G.; Paoli, G. S. M.; Salinas, G. L. R.; Chagoyan, H. S.; Floroentino, Z. A. S.; Calixto, E.; Figueroa, G. E. P.; Cater, R.; Melgoza, R. J.; Mattinez, B. S. R.; Soto, E. F. Theophylline: Old drug in a new light, application in COVID-19 through computational studies. *Int. J. Mol. Sci.* **2022**, *23*, 4167.
(15) Chikhale, R.; Sinha, S. K.; Wanjari, M.; Gurav, N. S.; Ayyana, M.; Prasad, S.; Khanal, P.; Dey, Y. N.; Patil, R. B.; Gurav, S. S. Computational assessment of saikosaponins as adjuvant treatment for COVID-19: molecular docking, dynamics, and network pharmacology analysis. *Mol. Diversity* **2021**, *25*, 1889−1904.
(16) Malone, B.; Urakova, N.; Snijder, E. J.; Combell, E. A. Structures and functions of coronavirus replication-transcription complexes and their relevance for SARS-CoV-2 drug design. *Nat. Rev. Mol. Cell Biol.* **2022**, *23*, 21−39.
(17) Qiao, J.; Li, Y. S.; Zeng, R.; Liu, F. L.; Luo, H. R.; Huang, C.; Wang, Y. F.; Zhang, J.; Quan, B.; Shen, C.; Mao, X.; Liu, X.; Sun, W.; Yang, W.; Ni, X.; Wang, K.; Xu, L.; Duan, Z. L.; Zou, Q. C.; Yang, S.; et al. SARS-CoV-2 M^{pro} inhibitors with antiviral activity in a transgenic mouse model. *Science* **2021**, *371* (6536), 1374−1378.
(18) Sobhia, M. E.; Ghosh, K.; Sivangula, S.; Kumar, S.; Singh, H. Identification of potential SARS-CoV-2 M^{pro} inhibitors integrating molecular docking and water thermodynamics. *J. Biomol. Struct. Dyn.* **2021**, *40* (11), 5079−5089.
(19) Kneller, D. W.; Phillips, G.; O'Neill, H. M.; Jedrzejczak, R.; Stols, L.; Langan, P.; Joachimiak, A.; Coates, L.; Kovalevsky, A. Structural plasticity of SARS-CoV-2 3CL M^{pro} active site cavity revealed by room temperature X-ray crystallography. *Nat. Commun.* **2020**, *11*, No. 3202.
(20) Rutwick Surya, U.; Praveen, N. A molecular docking study of SARS-CoV-2 main protease against phytochemicals of *Boerhavia diffusa* Linn. for novel COVID-19 drug discovery. *Virus Dis.* **2021**, *32*, 46−54.
(21) Peiris, M. Pathogenesis of avian flu H5N1 and SARS. *Innate Immun. Pulm. Infect.* **2006**, *279*, 56−65.
(22) Flerlage, T.; Boyd, D. F.; Meliopoulos, V.; Thomas, P. G.; Vherry, S. S. Influenza virus and SARS-CoV-2: pathogenesis and host responses in the respiratory tract. *Nat. Rev. Microbiol.* **2021**, *19* (7), 425−441.
(23) Abdelrahman, Z.; Li, M.; Wang, X. Comparative review of SARS-CoV-2, SARS-CoV, MERS-CoV and influenza A respiratory viruses. *Front. Immunol.* **2020**, *11*, No. 552909.
(24) Khorramdelazad, H.; Kazemi, M. H.; Najafi, A.; Keykhaee, M.; Emaneh, R. Z.; Falak, R. Immunopathological similarities between COVID-19 and influenza: Investigating the consequences of Co-infection. *Microb. Pathog.* **2021**, *152*, No. 104554.
(25) Khalilieh, S.; Yee, K. L.; Sanchez, R.; Stoch, S. A.; Wenning, L.; Iwamoto, M. Clinical pharmacokinetics of the novel HIV-1 non-nucleoside reverse transcriptase inhibitor doravirine: An assessment of the effect of patient characteristics and drug-drug interactions. *Clin. Drug Invest.* **2020**, *40*, 927−946.
(26) Nair, A. S.; Singh, A. K.; Kumar, A.; Kumar, S.; Sukumaran, S.; Koyiparambath, V. P.; Pappachen, L. K.; Rangarajan, T. M.; Kim, H.; Mathew, B. FDA-Approved trifluoromethyl group-containing drugs: A Review of 20 years. *Processes* **2022**, *10*, 2054.
(27) Ng, K. E. Xofluza (Baloxavir Marboxil) for the treatment of acute uncomplicated influenza. *Pharm. Ther.* **2019**, *44*, 9−11.
(28) El-Sayed, W. A.; Khalal, H. S.; Mohomed, S. F.; Hussien, H. A.; Kutkat, O. M.; Amer, A. E. Synthesis and antiviral activity of 1,2,3-triazole glycosides based substituted pyridine via click cycloaddition. *Russ. J. Gen. Chem.* **2017**, *87*, 2444−2453.
(29) Forrestall, K. L.; Burley, D. E.; Cash, M. K.; Pottie, I. R.; Darvesh, S. 2-Pyridone natural products as inhibitors of SARS-CoV-2 main protease. *Chem. Biol. Interact.* **2021**, *335*, No. 109348.
(30) Asiri, Y. I.; Alsayari, A.; Muhsinah, A. B.; Mabkhot, Y. N.; Hassan, M. Z. Benzothiazoles as potential antiviral agents. *J. Pharm. Pharm.* **2020**, *72*, 1459−1480.
(31) Scheetz, M. E.; Carlson, D. G.; Schinitsky, M. R. Frentizole, a novel immunosuppressive, and azathioprine: their comparative effects on host resistance to Pseudomonas aeruginosa, Candida albicans, herpes simplex virus, and influenza (Ann Arbor) virus. *Infect. Immun.* **1977**, *15* (1), 145−148.
(32) United states National library of Med. Chem. IDplus advanced: TMC-310911. https://clinicaltrials.gov/ct2/show/NCT 04261270.
(33) Haroun, M.; Tratrat, C.; Kositzi, K.; Tsolaki, E.; Petrou, A.; Aldhubiab, B.; Attimarad, M.; Harsha, S.; Geronikaki, A.; Venugopala, K. N.; Elsewedy, H. S.; Sokovic, M.; Glamoclija, J.; Ciric, A. New benzothiazole-based thiazolidinones as potent antimicrobial agents: Design, synthesis and biological evaluation. *Curr. Top. Med. Chem.* **2018**, *18*, 75−87.
(34) Kamat, V.; Santosh, R.; Poojary, B.; Nayak, S. P.; Kumar, B. K.; Sankaranarayanan, M.; Faheem; Khanapure, S.; Barretto, D. A.; Vootla, S. K. Pyridine- and Thiazole-Based Hydrazides with Promising Anti-inflammatory and Antimicrobial Activities along with Their *In Silico* Studies. *ACS Omega* **2020**, *5*, 25228−25239.
(35) Sharma, P. C.; Sinhmar, A.; Sharma, A.; Rajak, H.; Pathak, D. P. Medicinal significance of benzothiazole scaffold: an insight view. *J. Enzyme Inhib. Med. Chem.* **2013**, *28*, 240−266.
(36) Azzam, R. A.; Elboshi, H. A.; Elgemeie, G. H. Novel synthesis and antiviral evaluation of new benzothiazole-bearing *N*-sulfonamide 2-pyridone derivatives as USP7 enzyme inhibitors. *ACS Omega* **2020**, *5*, 30023−30036.
(37) Azzam, R. A.; Elsayed, R. E.; Elgemeie, G. H. Design and synthesis of a new class of pyridine-based *N*-sulfonamides exhibiting antiviral, antimicrobial, and enzyme inhibition characteristics. *ACS Omega* **2020**, *5*, 26182−26194.
(38) Azzam, R. A.; Elsayed, R. E.; Elgemeie, G. H. Design, synthesis, and antimicrobial evaluation of a new series of N-sulfonamide 2-pyridones as dual inhibitors of DHPS and DHFR enzymes. *ACS Omega* **2020**, *5*, 10401−10414.
(39) Elgemeie, G. H.; Azzam, R. A.; Osman, R. R. Recent advances in synthesis, metal complexes and biological evaluation of2-aryl, 2-pyridyl and 2-pyrimidylbenzothiazoles as potential Chemotherapeutics. *Inorg. Chim. Acta* **2020**, *502*, No. 119302.
(40) Metwally, N. H.; Deeb, E. A. Synthesis, anticancer assessment on human breast, liver and colon carcinoma cell lines and molecular modeling study using novel pyrazolo[4,3-*c*]pyridine derivatives. *Bioorg. Chem.* **2018**, *77*, 203−214.
(41) Metwally, N. H.; Badawy, M. A.; Okpy, D. S. Green synthesis of some new thio- pyrano[2,3-*d*][1,3]thiazoles using lemon juice and their antibacterial activity. *Synth. Commun.* **2018**, *48*, 2496−2509.
(42) Metwally, N. H.; Radwan, I. T.; El-Serwy, W. S.; Mohamed, M. A. Design, synthesis, DNA assessment and molecular docking study of

https://doi.org/10.1021/acsomega.3c01987
ACS Omega 2023, 8, 36636−36654

novel 2-(pyridin-2-ylimino) thiazolidin-4-one derivatives as potent antifungal agents. *Bioorg. Chem.* **2019**, *84*, 456−467.
(43) Metwally, N. H.; Mohamed, M. S.; Ragb, E. A. Design, synthesis, anticancer evaluation, molecular docking and cell cycle analysis of 3-methyl-4,7-dihydropyrazolo[1,5-*a*] pyrimidine derivatives as potent histone lysine demethylases (KDM) inhibitors and apoptosis inducers. *Bioorg. Chem.* **2019**, *88*, No. 102929.
(44) Almahdi, M. M.; Saeed, A. E. M.; Metwally, N. H. Synthesis and antimicrobial activity of some new pyrazoline derivatives bearing sulfanilamido moiety. *Eur. J. Chem.* **2019**, *10*, 30−36.
(45) Metwally, N. H.; Saad, G. R.; Abdwahab, E. A. Grafting of multiwalled carbon nanotubes with pyrazole derivatives: characterization, antimicrobial activity and molecular docking study. *Int. J. Nanomed.* **2019**, *14*, 6645−6659.
(46) Metwally, N. H.; Mohammed, M. S. New imidazolone derivatives comprising a benzoate or sulfonamide moiety as anti-inflammatory and antibacterial inhibitors: Design, synthesis, selective COX-2, DHFR and molecular-modeling study. *Bioorg. Chem.* **2020**, *99*, No. 103438.
(47) Metwally, N. H.; Abdallah, S. O.; Mohsen, M. M. A. Design, green one-pot synthesis and molecular docking study of novel *N, N*-bis(cyanoacetyl)hydrazines and bis-coumarins as effective inhibitors of DNA gyrase and topoisomerase IV. *Bioorg. Chem.* **2020**, *97*, No. 103672.
(48) Metwally, N. H.; Elgemeie, G. H.; Jones, P. G. Crystal structure of ethyl 2-(5-amino-1-benzenesulfonyl-3-oxo-2,3-dihydro-1H-pyrazol-2-yl)acetate. *Acta Crystallogr., Sect. E: Cryst. Commun.* **2020**, *76*, 481−483.
(49) Metwally, N. H.; Badawy, M. A.; Okpy, D. S. Synthesis, biological evaluation of novel thiopyrano[2,3-d]thiazoles incorporating arylsulfonate moiety as potential inhibitors of tubulin polymerization, and molecular modeling studies. *J. Mol. Struct.* **2022**, *1258*, No. 132648.
(50) Metwally, N. H.; Abd-Elmoety, A. S. Novel fluorinated pyrazolo[1,5-a]pyrimidines: In a way from synthesis and docking studies to biological evaluation. *J. Mol. Struct.* **2022**, *1257*, No. 132590.
(51) Metwally, N. H.; El-Dosoky, E. A. Novel thiopyrano[2,3-*d*]thiazole-pyrazole hybrids as potential nonsulfonamide human carbonic anhydrase IX and XII inhibitors: Design, synthesis, and biochemical studies. *ACS Omega* **2023**, *8*, 5571−5592.
(52) Abu-Zaied, M. A.; Mahmoud, N. M.; Elgemeie, G. H. Toward developing therapies against corona virus: synthesis and anti-avian influenza virus activity of novel cytosine thioglycoside analogues. *ACS Omega* **2020**, *5*, 20042−20050.
(53) Hebishy, A. M. S.; Salama, H. T.; Elgemeie, G. H. New route to the synthesis of benzamide-based 5-aminopyrazoles and their fused heterocycles showing remarkable anti-avian influenza virus activity. *ACS Omega* **2020**, *5*, 25104−25112.
(54) Abu-Zaied, M. A.; Mahmoud, N. M.; Elgemeie, G. H. Synthesis of novel pyrimidine thioglycosides as structural analogs of favipiravir (avigan) and their antibird flu virus activity. *Nucleosides, Nucleotides Nucleic Acids* **2021**, *40*, 336−356.
(55) Elgemeie, G. H.; El Maksoud, F. A. Nitriles in heterocyclic synthesis: Novel synthesis of pyrido[2,1-b]benzothiazoles, pyrimido-[6,1-b]benzothiazoles and pyrazolo[4,3-c]pyridazine derivatives. *Heterocycles* **1986**, *24* (2), 349−353.
(56) Azzam, R. A.; Osman, R. R.; Elgemeie, G. H. Efficient synthesis and docking studies of novel benzothiazole based pyrimidinesulfonamide scaffolds as new antiviral agents and Hsp90α inhibitors. *ACS Omega* **2020**, *5*, 1640−1655.
(57) Maruyama, T.; Kozai, S.; Yamasaki, T.; Witvrouw, M.; Pannecouque, C.; Balzarini, J.; Snoeck, R.; Andrei, G.; De Clercq, E. Synthesis and antiviral activity of 1,3-disubstituted uracils against HIV and HCMV. *Antiviral Chem. Chemother.* **2003**, *14*, 271−279.
(58) Ogo, N.; Oka, T.; Ando, T.; Arahata, S.; Ikegaya, A.; Takagi, H.; Ogo, N.; Owada, K.; Kawrmori, F.; Wang, Q.; Saif, L. J.; Asai, A. Discovery and synthesis of heterocyclic carboxamide derivatives as potent anti-norovirus agents. *Chem. Pharm. Bull.* **2016**, *64*, 465−575.
(59) Dong, L.; Hu, S.; Goa, J. Discovering drugs to treat coronavirus disease 2019 (COVID-19). *Drug Discovery Ther.* **2020**, *14*, 58−60.
(60) Singh, A. K.; Singh, A.; Shaikh, A.; Singh, R.; Misra, A. Chloroquine and hydroxychloroquine in the treatment of COVID-19 with or without diabetes: A systematic search and a narrative review with a special reference to India and other developing countries. *Diabetes Metab. Syndr.: Clin. Res. Rev.* **2020**, *14*, 241−246.
(61) Dai, W.; Zhang, B.; Jiang, X. M.; Su, H.; Li, J.; Zhao, Y.; Xie, X.; Jin, Z.; Peng, J.; Liu, F.; Li, C.; Li, Y.; Bai, F.; Wang, H.; Cheng, X.; Cen, X.; Hu, S.; Yang, X.; Wang, J.; Liu, X.; Xiao, G.; Jiang, H.; Rao, Z.; Zhang, L. K.; Xu, Y.; Yang, H.; Liu, H. Structure-based design of antiviral drug candidates targeting the SARS-CoV-2 main protease. *Science* **2020**, *368*, 1331−1335.
(62) Ma, C.; Sacco, M. D.; Hurst, B.; Townsend, J. A.; Hu, Y.; Szeto, T.; Zhang, X.; Tarbet, B.; Marty, M. T.; Chen, Y.; Wang, J. Boceprevir, GC-376, and calpain inhibitors II, XII inhibit SARS-CoV-2 viral replication by targeting the viral main protease. *Cell Res.* **2020**, *30*, 678−692.
(63) Mosmann, T. Rapid colorimetric assay for cellular growth and survival: application to proliferation and cytotoxicity assays. *J. Immunol. Methods* **1983**, *65*, 55−63.
(64) Payne, S. Chapter 4 - Methods to study viruses. *Viruses* **2017**, 37−52.
(65) Hayden, F. G.; Cote, K. M.; Douglas, R. G., Jr Plaque inhibition assay for drug susceptibility testing of influenza viruses. *Antimicrob. Agents Chemother.* **1980**, *17*, 865−870.
(66) Feoktistova, M.; Geserick, P.; Leverkus, M. Crystal Violet Assay for Determining Viability of Cultured Cells. *Cold Spring Harbor Protoc.* **2016**, *2016* (4), No. pdb.prot087379, DOI: 10.1101/pdb.prot087379.
(67) Zhang, J.; Zhan, B.; Yao, X.; Gao, Y.; Song, J. Antiviral activity of tannin from the pericarp of punica granatum L. against genital herpes virus in vitro. *Zhongguo Zhong Yao Za Zhi* **1995**, *20*, 556−558.
(68) Kuo, Y. C.; Lin, L. C.; Tsai, W. J.; Chou, C. J.; Kung, S. H.; Ho, Y. H. Samarangenin b from Limonium sinense suppresses herpes simplex virus type 1 replication in Vero cells by regulation of viral macromolecular synthesis. *Antimicrob. Agents Chemother.* **2002**, *46*, 2854−2864.
(69) Schuhmacher, A.; Reichling, J.; Schnitzler, P. Virucidal effect of peppermint oil on the enveloped viruses herpes simplex virus type 1 and type 2 in vitro. *Phytomedicine* **2003**, *10*, 504−510.

https://doi.org/10.1021/acsomega.3c01987
ACS Omega 2023, 8, 36636−36654